

1 **Non-Stationary Dynamics of Compound Climate Extremes: A WRF-CMIP6-**
2 **GAMLSS Framework for Southeastern China**

3 Yinchi Zhang^{1, 2, 3, 4}, Wanling Xu⁵, Chao Deng⁶, Shao Sun⁷, Miaomiao Ma⁸, Jianhui Wei¹⁰, Ying
4 Chen^{1, 2, 3, 9}, Yi Wang⁴, Lu Gao^{1, 2, 3, 9*}, Harald Kunstmann^{10, 11, 12}

5 ¹*Key Laboratory for Humid Subtropical Eco-geographical Processes of the Ministry of Education,*
6 *Fujian Normal University, Fuzhou, 350117, China*

7 ²*Institute of Geography, Fujian Normal University, Fuzhou, 350117, China*

8 ³*School of Geographical Science, Fujian Normal University, Fuzhou, 350117, China*

9 ⁴*Department of Geography and School of Global Studies, University of Sussex, Falmer, Brighton*
10 *BN1 9RH, UK*

11 ⁵*School of Ocean and Earth Science, Tongji University, Shanghai, 200092, China*

12 ⁶*Sichuan Academy of Forestry Sciences, Chengdu, 610081, China*

13 ⁷*State Key Laboratory of Severe Weather, Chinese Academy of Meteorological Sciences, Beijing*
14 *100081, China*

15 ⁸*China Institute of Water Resources and Hydropower Research, Beijing, 100038, China*

16 ⁹*Fujian Provincial Engineering Research Center for Monitoring and Accessing Terrestrial*
17 *Disasters, Fujian Normal University, Fuzhou, 350117, China*

18 ¹⁰*Institute of Meteorology and Climate Research (IMKIFU), Karlsruhe Institute of Technology,*
19 *Campus Alpin, Garmisch-Partenkirchen, Germany*

20 ¹¹*Institute of Geography, University of Augsburg, Augsburg, 86159, Germany*

21 ¹²*Centre for Climate Resilience, University of Augsburg, Augsburg, 86159, Germany*

22 ***Corresponding Author: Lu Gao, l.gao@foxmail.com**

23 **Abstract**

24 Understanding future changes in compound climate extremes (CCEs) is critical for climate
25 risk assessment. Existing research, however, has largely relied on stationary assumptions,
26 overlooking the dynamic evolution of CCEs under non-stationary climate change. To address this
27 gap, this study employs an enhanced Generalized Additive Model for Location, Scale, and Shape
28 (GAMLSS) framework to provide novel insights into the non-stationary characteristics of hot-wet
29 (HW), hot-dry (HD), cold-wet (CW), and cold-dry (CD) extremes under future climate scenarios.
30 We focus on the Minjiang River Basin (MRB) in Southeast China. A high-resolution dataset for
31 CEE detection was generated by dynamical downscaling a bias-corrected CMIP6 dataset, using the
32 Weather Research and Forecasting (WRF) model. Our results indicate that (1) CCEs increase
33 significantly at a rate of 3.55 days per decade under the SSP5-8.5 scenario, with hot extremes (HW
34 and HD) being the dominant contributors. Spatially, the increases exhibit a distinct west to east
35 gradient, peaking in the downstream areas of the MRB. (2) Under the SSP5-8.5 scenario, CCEs
36 exhibit a marked shift from stationary to non-stationary characteristics, with non-stationarity
37 detected in 95.20% of grid cells. This transition is primarily driven by mean warming, which
38 explains 80.81% of the change, rather than by variability. (3) The non-stationary results demonstrate
39 that the severity and recurrence frequency of CCEs are systematically underestimated under
40 stationary assumptions. Most CCE types (except for CD) show an increasing recurrence frequency
41 under the SSP5-8.5 scenario. For instance, the frequency of events with a 100-year return period
42 increases at a stronger trend of 3.12 days per decade. This study emphasizes the necessity of
43 updating the frequency changes of CCEs under a non-stationary framework.

44 **Keywords** compound climate extremes, non-stationarity, GAMLSS, dynamical downscaling, WRF

45 **1 Introduction**

46 Global warming is leading to more frequent and intense compound climate extremes (CCEs)
47 (Sauter et al., 2023; Liu et al., 2024; Zhang et al., 2024; You et al., 2025). CCEs have posed severe
48 threats to global social, economic, and ecological systems, with impacts that surpass those of
49 individual extremes in both range and severity (Mukherjee et al., 2023; Zeng et al., 2024; Miao et
50 al., 2024). For example, the Yangtze River Basin in China experienced unprecedented compound
51 hot-dry extremes in August 2022, characterized by record-breaking heatwaves and severe droughts,
52 which directly affected over 50 million people (Jia et al., 2025). The Sixth Intergovernmental Panel
53 on Climate Change (IPCC) report indicated that the probability and intensity of future CCEs are
54 projected to increase (IPCC, 2021). Therefore, a systematic assessment of the future evolution of
55 CCEs is critical for mitigating socio-economic risks and optimizing climate adaptation strategies.

56 Recent studies have increasingly focused on CCEs, highlighting their growing significance in
57 the context of climate change. Zscheischler et al. (2018) were the first to clearly define the concept
58 of compound events, emphasizing how the interaction of multiple climate and meteorological
59 drivers can amplify extreme impacts. Building on this, Ridder et al. (2022) conducted the first
60 global-scale assessment of the changes in compound events, specifically examining the co-
61 occurrence of heatwaves and drought, extreme winds, and precipitation. Wu et al. (2023) revealed
62 that under warming conditions, the risks associated with global compound pluvial–hot extreme
63 events are projected to be significantly greater in the future than those observed during the historical
64 period. Fang et al. (2025) investigated the future changes of sequential heatwaves and precipitation
65 events as well as concurrent drought and heatwave events in China, with projections indicating an
66 increase in both the frequency and intensity of these events.

67 While large-scale studies play a crucial role in advancing our understanding of global climate
68 change and extreme events, their practical relevance for disaster risk management and adaptation
69 strategies in medium- and small-scale regions is relatively limited due to their lower spatial and
70 temporal resolution. To overcome this constraint, dynamical downscaling, which utilizes nested
71 high-resolution regional climate models (RCMs), provides a critical technical pathway to
72 investigate climate response mechanisms at fine-scales (Tapiador et al., 2020; Rahimi et al., 2024).
73 Compared to Global Climate Models (GCMs), RCMs offer higher spatial resolution, allowing for

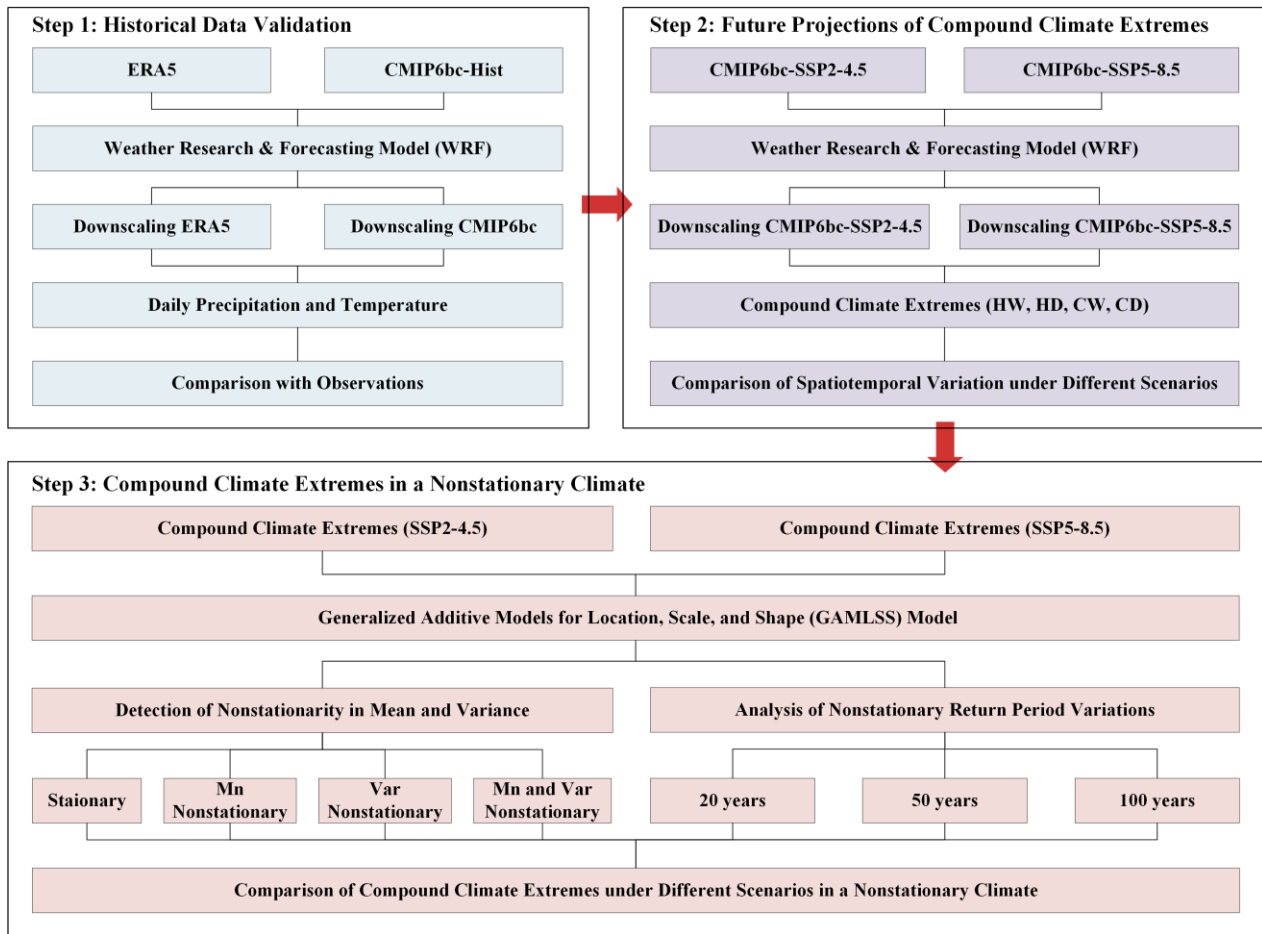
74 more precise simulations of local climate effects induced by topography, such as local convective
75 precipitation, orographic effects, and regional climate heterogeneity (Gilbert et al., 2025). In regions
76 with complex terrain, RCMs are particularly effective at capturing spatial variations of climate
77 variables, such as the differences in wind patterns, precipitation, and their distribution caused by
78 topography in mountainous or basin areas (Imran and Evans, 2025). For example, Byun et al. (2023)
79 assessed the ability of RCMs and GCMs to simulate storm tracks in East Asia, revealing that RCMs
80 are better able to capture high-resolution topography, thereby reducing the biases found in GCMs.
81 Lin et al. (2022) showed that RCMs driven by ERA-Interim reanalysis data are capable of capturing
82 small-scale processes, such as orographic effects, and outperform GCMs in reproducing the large-
83 scale features of the Heat Wave Magnitude Index-daily. Torrez-Rodriguez et al. (2023) also
84 demonstrated that RCMs are better at reproducing the main spatio-temporal characteristics of
85 precipitation in subtropical complex terrain regions. As an advanced convection-permitting RCM,
86 the WRF model significantly enhances the simulation capability for meteorological processes at 1-
87 10 km scales through its fully compressible, non-hydrostatic dynamic core framework (Talbot et
88 al., 2012). This high-resolution simulation capability gives the WRF model a unique advantage in
89 capturing small-scale meteorological phenomena. Zhou et al. (2024) developed a 9 km resolution
90 regional reanalysis dataset covering the Tibetan Plateau based on the WRF model, and
91 demonstrated its superior applicability compared to the fifth generation European Centre for
92 Medium-Range Weather Forecasts Reanalysis (ERA5). Yang et al. (2024) revealed that the WRF
93 model provides better accuracy in simulating snow depth during the cold season in high-elevation
94 regions compared to ERA5-Land.

95 Additionally, traditional extreme event analyses rely on stationarity assumptions (when
96 analyzing time series data, it is assumed that the statistical properties of the series remain constant
97 over time), presuming that the probability and distributional parameters of climate variables are
98 constant (Sun et al., 2018; Nerantzaki et al., 2023). However, driven by synergistic effects of global
99 warming and anthropogenic forcing, extremes exhibit significant shifts in distributional
100 characteristics (Gao et al., 2018). Therefore, traditional models fail to capture the non-stationary
101 (the statistical properties of a time series change over time and do not remain constant) changes in
102 these extreme events. Many studies have applied the Generalized Additive Models for Location,

103 Scale, and Shape (GAMLSS) (Rigby and Stasinopoulos 2005) to address non-stationary problems
104 in hydrological and meteorological extremes, enabling updated risk analysis of evolving climate
105 extremes. Lei et al. (2021) investigated the non-stationary changes of extreme precipitation in the
106 Poyang Lake Basin and found that the stationary assumption underestimates the intensity of
107 extreme precipitation in this region. Shao et al. (2022) innovatively proposed the Nonstationary
108 Standardized Runoff Index (NSRI), and the results indicate that, compared to the stationary index,
109 it can more accurately identify drought events. Salarijazi et al. (2023) evaluated the nonstationarity
110 of maximum temperatures in multiple urban areas of Iran and concluded that traditional stationary
111 approaches tend to underestimate the risk of annual maximum temperatures. However, existing
112 non-stationary analyses only focus on individual extremes, and the potential non-stationarity of
113 CCEs has not been established. The comprehensive assessment of future changes in CCEs within
114 a non-stationary framework is also lacking.

115 To address these research gaps, this study adopts a high-resolution approach by integrating the
116 WRF model with GAMLSS. We first perform dynamical downscaling using the WRF model to
117 refine the bias-corrected Coupled Model Intercomparison Project Phase 6 (CMIP6bc) data (1.25°
118 $\times 1.25^\circ$) to a 3 km resolution. Based on these high-resolution WRF outputs, CCEs are then
119 identified and used as input for the GAMLSS framework to analyze their non-stationary
120 characteristics. This methodology overcomes the limitations of traditional coarse-resolution models
121 and addresses the shortcomings of stationary assumptions in CCE analysis. By focusing on the
122 Minjiang River Basin (MRB)—a subtropical, monsoon-dominated basin in southeastern China
123 where complex topographic-climatic interactions give rise to high-intensity compound
124 hydroclimatic extremes (Gan et al., 2025; Geng et al., 2024; Wang et al., 2024)—this research aims
125 to examine four types of CCEs: hot-wet (HW), hot-dry (HD), cold-wet (CW), and cold-dry (CD)
126 events. The analysis proceeds as follows (Figure 1): Supplement Section S1 presents the validation
127 of CMIP6bc applicability. Section 3.1 characterizes the spatio-temporal patterns of CCEs under
128 both a middle-of-the-road scenario (SSP2-4.5) and a high-emissions scenario (SSP5-8.5). The non-
129 stationarity detection of CCEs is described in Section 3.2. The recurrence frequency changes in
130 CCEs under non-stationary conditions is evaluated in Section 3.3. The work establishes a scientific
131 basis for addressing the environmental and climatic challenges posed by CCEs, thereby

132 contributing to effective strategies for regional sustainability and climate resilience.



133

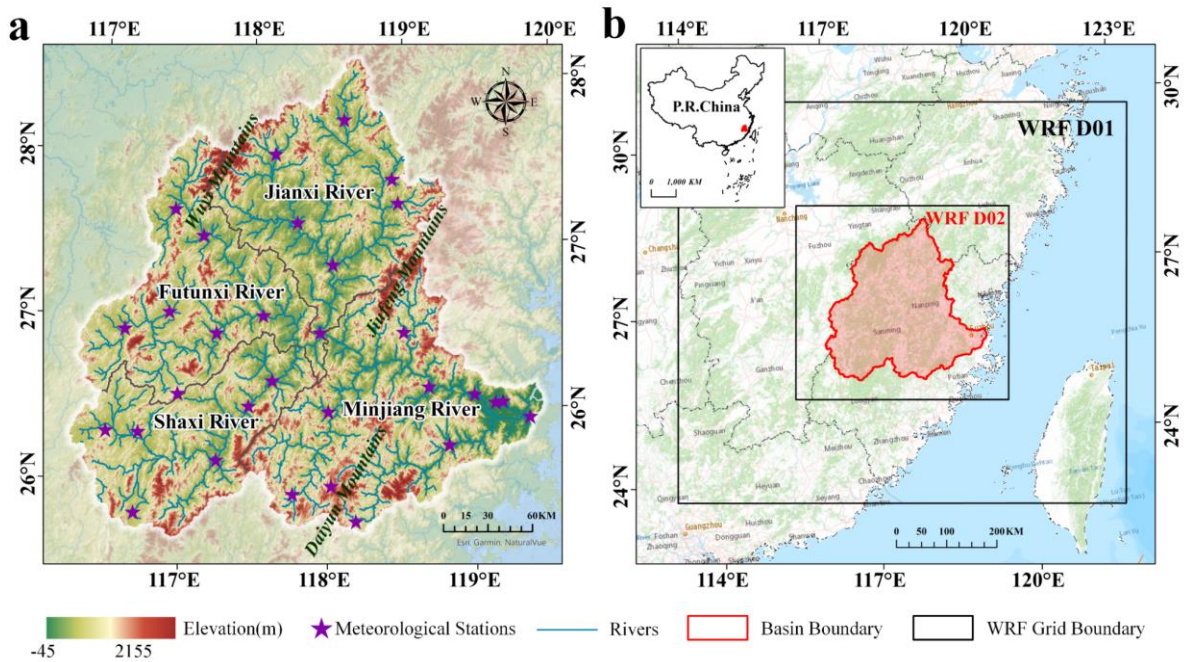
134 Figure 1. Flowchart of CCEs projection in a non-stationary framework.

135 **2 Study region, methods and data**

136 **2.1 Study region**

137 The MRB is a complex topographic basin in southeastern coastal China (Figure 2a). The
 138 Minjiang River, the main stream of the basin, drains an area of 60,992 km²—accounting for nearly
 139 half Fujian Province's territory. Encompassing three principal tributaries (Jianxi, Futunxi, and Shaxi
 140 rivers), the MRB experiences a subtropical monsoon climate characterized by 1700 mm mean
 141 annual precipitation and 18°C mean temperature. (Zheng et al., 2023). The basin displays spatio-
 142 temporal heterogeneity in precipitation, with flood seasons from April to September that often
 143 accompany CCEs. Particularly in the late flood season (July to September), the MRB experiences
 144 frequent typhoon-related compound disasters: the upper and middle reaches are commonly affected
 145 by typhoon-rainstorm-landslide events, while the lower reaches face high occurrences of typhoon-
 146 rainstorm-urban waterlogging and typhoon-rainstorm-flood events (Yang et al., 2025). In 2023, for

147 example, typhoon Doksuri (No. 2305) caused approximately 66,794 people to be affected in Fuzhou,
 148 the downstream city of the MRB, with direct economic losses reaching 588 million RMB (Yan et
 149 al., 2024). In addition, the region also exhibits a climate characteristic of concurrent rainfall and
 150 heat, with CCEs frequently occurring during the warm season, driven by high temperature and
 151 heavy rainfall (Sun et al., 2025).



152
 153 Figure 2. Study area and model configuration. (a) Topographic features of the MRB (m) and (b)
 154 Model configuration with 9-km (D01) and 3-km (D02) nested domains (Zhang et al., 2025).
 155 Basemap source: © Esri, <https://services.arcgisonline.com>

156 2.2 Data

157 Obtained from the Science Data Bank, the CMIP6bc dataset serves as the foundation for this
 158 investigation (Xu et al., 2021, <https://www.scidb.cn>), which is constructed using the ERA5. This
 159 dataset incorporates an 18-model CMIP6 ensemble mean (Supplement Table S1), maintaining both
 160 climatological mean and interannual variability statistics while preserving nonlinear temporal
 161 trends. Compared with original CMIP6 data, CMIP6bc demonstrates superior performance in
 162 extreme event simulation. Despite its widespread application in previous studies (Jamal et al., 2023;
 163 Huang et al., 2024; Wu and Zheng, 2023), we conduct a 10-year validation over the MRB.
 164 Considering both the reliability of the dataset and the need to optimize computational resources
 165 (simulating one year over the MRB requires approximately four days on 80 CPU cores), we select

166 a 10-year historical period (2005–2014) as sufficient to demonstrate the reliability of the CMIP6bc
 167 dataset for driving the WRF simulations. ERA5, as a widely used WRF-driven dataset (Arnault et
 168 al., 2021; Jiang et al., 2021; Varga and Breuer, 2022; Shang et al., 2022), is utilized here as a
 169 reference for the simulation results. Fujian Provincial Meteorological Bureau provides daily
 170 precipitation and temperature records from its 30 monitoring stations, which are used as validation
 171 data for this study. Future scenarios under SSP2-4.5 and SSP5-8.5 (2025–2065) are employed to
 172 project future changes in CCEs.

173 **2.3 WRF model setup**

174 This research utilizes the WRF Version 4.3 with two-domain nested configuration, featuring
 175 grid spacings of 9 km and 3 km (Figure 2b). Table 1 summarizes the optimal physics
 176 parameterization schemes selected through our comprehensive sensitivity experiments
 177 (Supplement Result S2) (Lin et al., 2023; Zhang et al., 2025). At sufficiently high model resolutions,
 178 deep convective processes can be explicitly resolved (Arakawa and Jung, 2011). Therefore, the
 179 cumulus parameterization scheme is deactivated in the inner domain (D02) to leverage convection-
 180 permitting capability. We first simulate daily precipitation and temperature over the MRB from
 181 January 1, 2005 to December 31, 2014, using both CMIP6bc and ERA5 forcing data. Subsequently,
 182 future projections from January 1, 2025 to December 31, 2065 are conducted using CMIP6bc under
 183 two climate projection scenarios.

184 Table 1 Settings for WRF model in this study.

WRF model setup overview		Parameterization scheme settings	
Forcing data	CMIP6bc, ERA5	Microphysics	Purdue Lin (Chen and Sun, 2002)
Centre	118.02E°, 26.83N°	Cumulus convection	New Tiedtke (Zhang et al., 2011)
Grid	100×90, 142×130	Longwave radiation	RRTMG (Mlawer et al., 1997)
Resolution	9km, 3km	Shortwave radiation	Dudhia (Dudhia, 1989)
E_vert	45	Boundary layer	YSU (Hong et al., 2006)
Spin-up time	7 days	Land surface	Noah-MP (Niu et al., 2011)

185 **2.4 Definition of CCEs**

186 This study considers four types of CCEs: hot-wet events (HW), hot-dry events (HD), cold-wet
 187 events (CW) and cold-dry events (CD). We adopt the widely used thresholds (the 90th and 10th
 188 percentiles) to identify CCEs (Croitoru et al., 2016; Song et al., 2019; Patel et al., 2024). We first
 189 extract daily precipitation (>0.1 mm) and temperature data for each grid during 2025-2065, defining

190 the 90th and 10th percentiles as thresholds to identify hot/cold and wet/dry extremes, respectively.
 191 Specifically, we define extreme temperature events as occurring when daily temperatures are higher
 192 (hot extremes) or lower (cold extremes) than the threshold. Wet events are characterized by rainfall
 193 surpassing the threshold (90th), while dry events are characterized by seven consecutive days
 194 without rainfall. For dry conditions defined as seven consecutive days without precipitation, each
 195 day within a dry spell is treated as a dry day in the counting of CCEs. We conduct calculations
 196 independently for each grid point, applying thresholds specific to each point. Specifically, for
 197 interannual variation, we sort the precipitation and temperature data over a 40-year period and
 198 determine the thresholds based on the 10th and 90th percentiles to identify CCEs. For seasonal
 199 variations, we separately extract the precipitation and temperature data for the summer (JJA) and
 200 winter (DJF) seasons, applying the same sorting method to calculate the respective thresholds, thus
 201 analyzing the distribution characteristics of CCEs for each season.

202 **2.5 GAMLSS model**

203 GAMLSS is a flexible statistical model used for analyzing distributions with non-stationary
 204 characteristics (Rigby and Stasinopoulos, 2005). It extends the traditional generalized linear models
 205 (GLMs) and generalized additive models (GAMs) by introducing joint modeling of all distribution
 206 parameters (location, scale, and shape). Unlike traditional regression models, GAMLSS effectively
 207 characterizes both linear and nonlinear dependencies linking predictors to response variables. (D.
 208 M. Stasinopoulos and Rigby, 2007).

209 This study employs the semi-parametric GAMLSS, which accommodates parametric terms,
 210 nonparametric smooth functions, and random effects within a unified modeling structure (Gao et
 211 al., 2018). Consider z independent samples $y_i (i = 1, \dots, z)$ following a distribution $F_y(y_i | \theta_i)$,
 212 where the parameter vector $\theta_{iT} = (\theta_{i1}, \theta_{i2}, \dots, \theta_{ik})$ contains k components representing location
 213 (Mn), scale (Var), and shape (skewness and kurtosis), with k normally not exceeding 4. Model
 214 selection is performed using Akaike's Information Criterion (AIC) (Akaike, 1974), with the optimal
 215 configuration identified through minimum AIC values., and model fitting quality is assessed by the
 216 Filliben correlation coefficient (Filliben, 1975). The GAMLSS is formally defined as follows:

$$217 \quad g_k(\theta_k) = \phi_k \beta_k + \sum_{j=1}^{j_k} h_{j_k}(x_{j_k})$$

218 where k denotes the indicator of distribution parameters, θ_k is the distribution parameter vector,
219 Φ_k represents $n \times j_k$ matrix of covariate variables, β_k is the coefficient vector of length j_k . $g_k(\cdot)$
220) is the link function connecting distribution parameter to linear predictor. $h_{j_k}(\cdot)$ defines how the
221 distribution parameter varies with covariate variable x_{j_k} . In the GAMLSS model, time (year) is
222 used as the independent variable (x), and the number of days per year for each type of CCE is
223 treated as the dependent variable (y), thereby enabling the calculation of the non-stationary
224 characteristics of each CCE. We employ two types of GAMLSS models to capture potential changes
225 in the distribution of meteorological variables. The first is the traditional two-parameter location–
226 scale model (mean μ and variance σ), which assumes a fixed distributional shape. The second is a
227 more flexible four-parameter location–scale–shape model (mean μ , variance σ , skewness v , and
228 kurtosis τ), allowing the distributional shape to evolve over time. These extended models retain the
229 mean and variance parameters while incorporating two additional shape parameters to capture
230 asymmetry and tail behavior. We assess the models by comparing their goodness of fit and select
231 the one that best represents the data distribution for subsequent analyses. Regarding the calculation
232 of stationarity, we consider the CCEs to be stationary if both the mean and variance remain stable.
233 If either the mean or variance shows significant variation, the CCEs are considered non-stationary.
234 Supplement Table S2 lists all the distribution functions implemented in our study. The R code for
235 implementing GAMLSS model can be accessed at <https://github.com/gamlss-dev/gamlss>.

236 **3 Results**

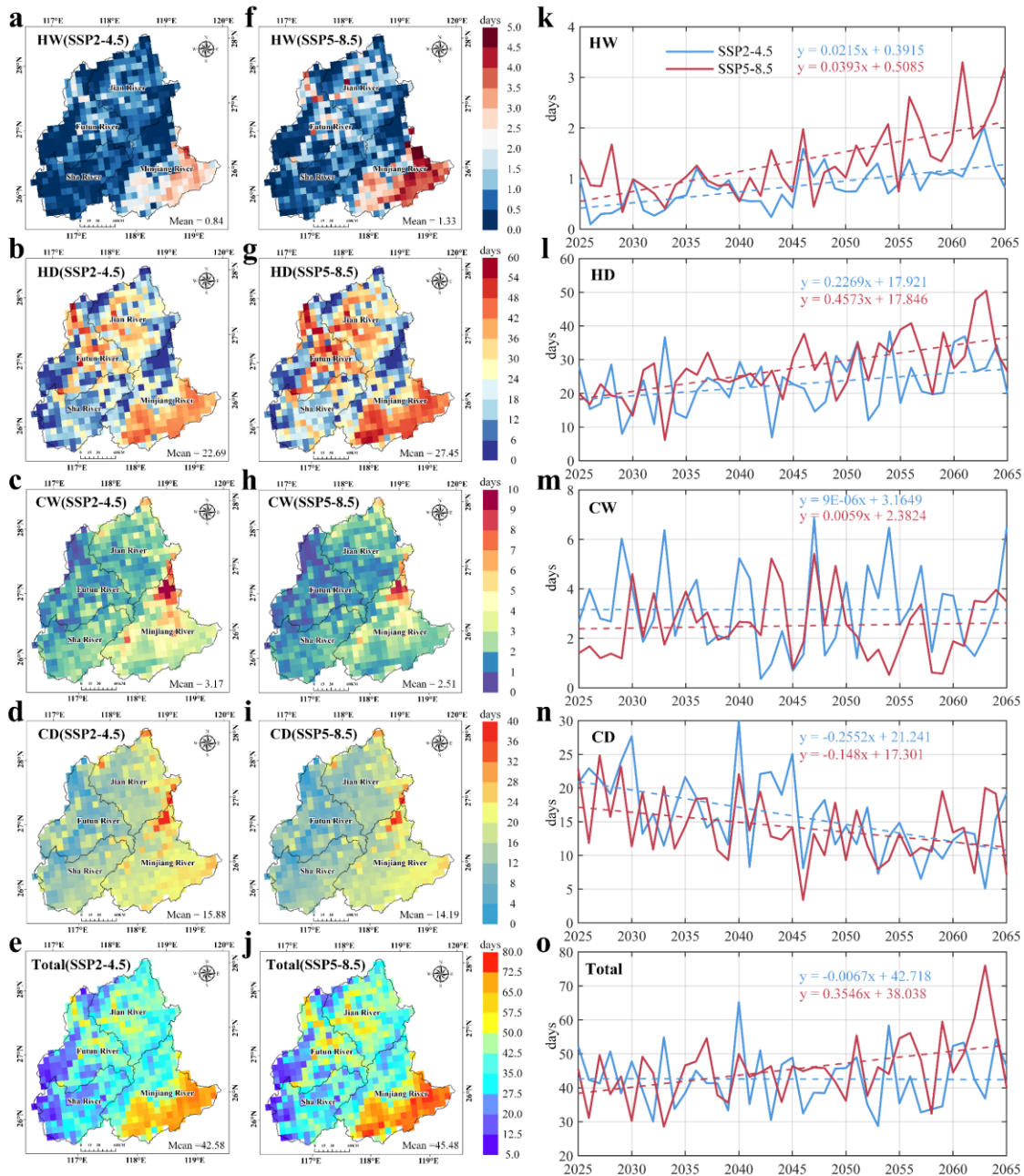
237 **3.1 Spatio-temporal patterns of CCEs under future scenarios**

238 Figures 3 (a–j) illustrate the spatial distribution of annual CCEs over the MRB during 2025–
239 2065. Overall, total CCEs are higher under the SSP5-8.5 scenario (45.48 days) than under the SSP2-
240 4.5 scenario (42.58 days). Dry-related extremes (HD and CD) dominate across the basin, whereas
241 wet-related extremes (HW and CW) are less frequent. Both hot extremes occur more frequently
242 under SSP5-8.5 than SSP2-4.5: HW increases from 0.84 to 1.33 days, and HD rises from 22.69 to
243 27.45 days. In contrast, cold extremes decrease: CW declines from 3.17 to 2.15 days, and CD from
244 15.88 to 14.19 days.

245 Spatially, the two scenarios exhibit similar geographic patterns. The highest frequencies
246 occurring in downstream regions, particularly for HD and HW. HD shows a wider spatial extent,

247 extending into the Futun River and Jian River Basins. Meanwhile, CW and CD display a clear west-
 248 to-east increasing gradient, with the highest values concentrated near the Jiufeng Mountains.

249 Temporally (Figures 3 k–o), CCE trends diverge sharply between scenarios. Under high-
 250 emission SSP5-8.5, total CCEs increase significantly at 3.55 days per decade, whereas SSP2-4.5
 251 projects stabilized frequencies. Hot extremes (HW and HD) increase more rapidly under SSP5-8.5,
 252 at rates nearly double those under SSP2-4.5. Conversely, the decline in CD is stronger under SSP2-
 253 4.5—approximately 1.7 times that under SSP5-8.5.

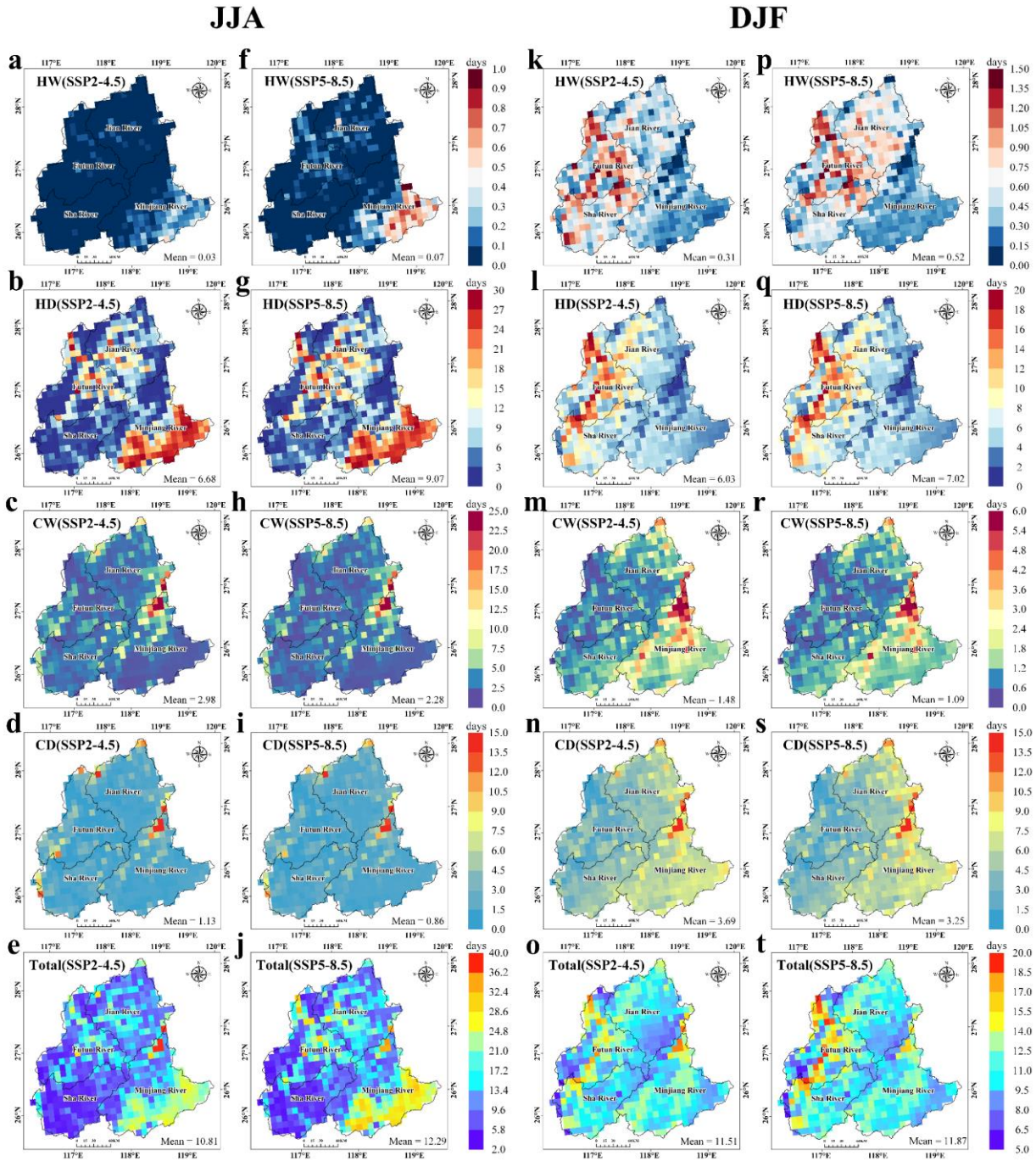


254
 255 Figure 3. Annual Spatio-temporal patterns of CCEs across the MRB from 2025 to 2065.

256 Building on the analysis of annual changes, we further investigate the seasonal variations of
257 CCEs. As shown in Figures 4 (a–j), the spatial distribution of summer CCEs largely resembles the
258 annual pattern, except for HW, which remain infrequent in this season. Nonetheless, a marked
259 increase in HW under the SSP5-8.5 is observed in the downstream MRB. In summary, total CCEs
260 increase during summer under both scenarios, rising more rapidly under SSP5-8.5 (2.26 days per
261 decade) than under SSP2-4.5 (0.79 days per decade). Moreover, differences between scenarios are
262 more pronounced for hot-related extremes (HW and HD) in summer than on the annual scale,
263 whereas cold-related events (CW, CD) show consistent patterns (Figures 5 a–e).

264 In winter, CCEs exhibit a contrasting spatial distribution (Figures 4 k–t). They occur
265 predominantly in the western MRB, particularly concentrated in the Futun River Basin, with higher
266 frequencies under SSP5-8.5 (11.87 days) than under SSP2-4.5 (11.51 days). This shift is primarily
267 driven by hot-related extremes (HW and HD), which move from the downstream MRB toward
268 western mountainous areas. Meanwhile, cold-related extremes (CW and CD) remain most frequent
269 in the Jiufeng Mountain areas. Winter CCEs show an increasing trend under SSP5-8.5 (0.76 days
270 per decade) but a slight decreasing trend under SSP2-4.5 (Figures 5 f–j). Among individual event
271 types, wet-related extremes (CW and HW) show insignificant trends, whereas HD increases (1.18
272 and 0.46 days per decade under SSP5-8.5 and SSP2-4.5, respectively) and CD decreases (–0.50 and
273 –0.70 days per decade under the two scenarios).

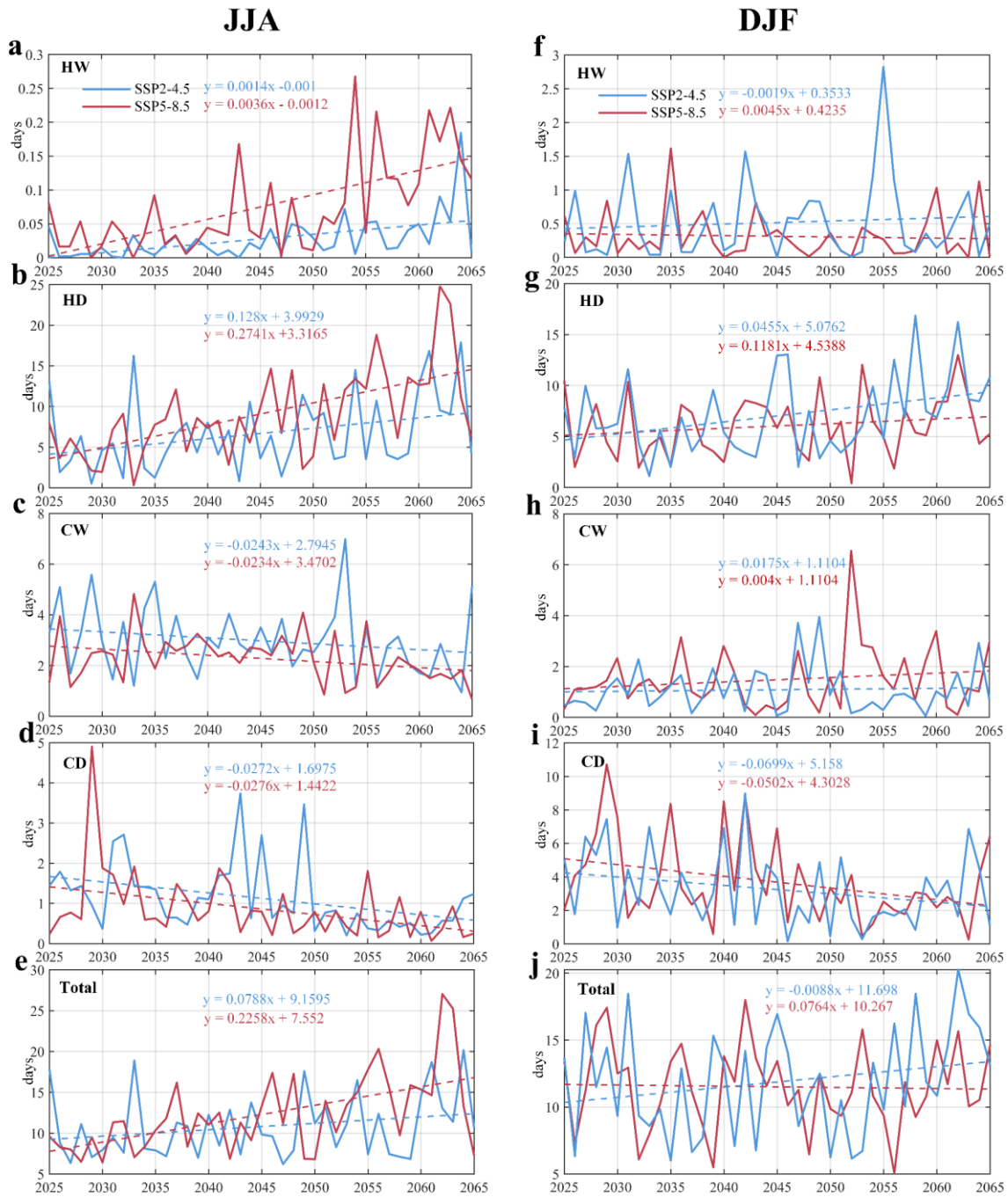
274 Given the importance of precipitation and temperature as key climate indicators, we calculate
275 their basin-averaged annual values and interannual trends. (Supplement Figure S5). Precipitation
276 varies only slightly, maintaining relatively stable annual fluctuations. In contrast, temperature
277 shows a distinct upward trend, which accelerates under high-emission SSP5-8.5 conditions (0.46°C
278 per decade). These results suggest that changes in CCEs across the MRB are primarily governed
279 by temperature-driven physical processes — where intensifying hot extremes coincide with
280 declining cold extremes—a conclusion supported by earlier studies (Wu et al., 2020; Zhao et al.,
281 2024; Duan et al., 2024).



282

283 Figure 4. Spatial patterns of CCEs in summer (JJA) and winter (DJF) across the MRB from 2025

284 to 2065.



285

286 Figure 5. Temporal patterns of CCEs in summer (JJA) and winter (DJF) across the MRB from 2025

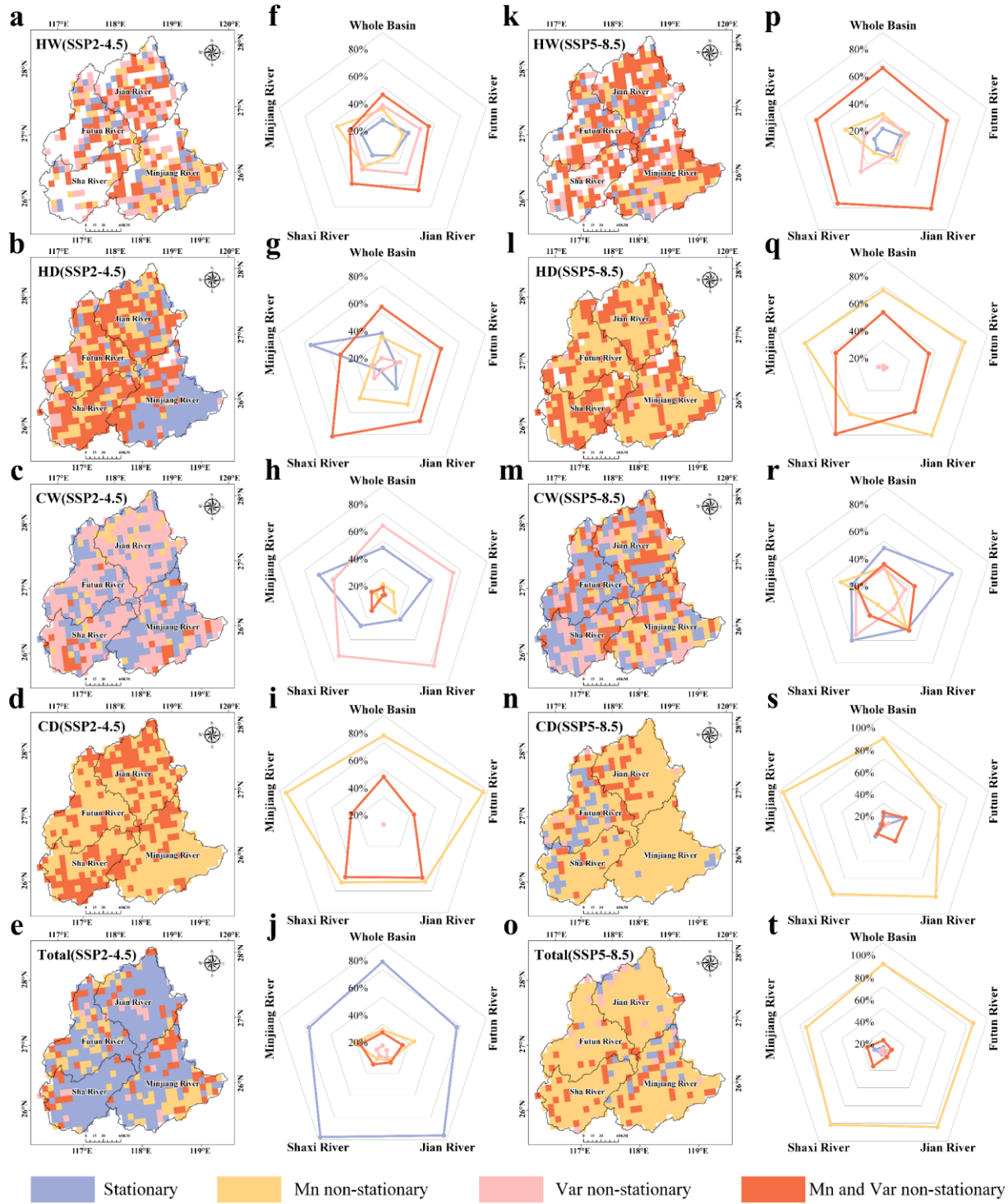
287 to 2065.

288 3.2 Non-stationary characteristics of CCEs

289 To quantify the non-stationary characteristics of CCEs, we analyze variations in both the mean
290 (Mn) and variance (Var) using GAMLSS (Figure 6). The model demonstrates excellent fitting
291 performance for all indices except HW, as indicated by Filliben coefficients exceeding 0.95 in
292 Supplement Figure S6.

293 Our results reveal a pronounced shift from stationary to non-stationary behavior in CCEs under
294 SSP5-8.5 compared to SSP2-4.5. This shift is primarily driven by non-stationarity in Mn, which
295 governs 80.81% of grid cells across the MRB. An additional 11.07% of grids are influenced by the
296 combined effects of both Mn and Var, primarily distributed in the Shaxi River Basin and the
297 downstream MRB. Dry-related extremes (HD and CD) show a transition from Var to Mn non-
298 stationarity. For HD, the area dominated by Mn non-stationarity expands from 22.65% to 57.03%
299 of grids, becoming the prevailing pattern (covering 60% of grids) in downstream regions where
300 stationarity was previously dominant (54.71%). Similarly, Mn non-stationarity for CD expands to
301 cover nearly the entire downstream MRB. For wet-related extremes (HW and CW), both Mn and
302 Var non-stationarity increase notably. The area dominated by Mn non-stationarity for HW rises
303 from 34.30% to 54.02% of grids, while for CW, it undergoes a more substantial increase from 0.06%
304 to 23.25%. Overall, CCEs under SSP5-8.5 display more widespread non-stationarity, with dry-
305 related extremes primarily governed by changes in Mn, whereas wet extremes are influenced by a
306 combination of Mn and Var effects.

307 Figure 7 further details the spatial patterns of Mn and Var in CCEs. Compared to Var, Mn
308 exhibits more pronounced and spatially extensive variations. For hot-related extremes (HW and
309 HD), Mn increases significantly across the entire basin under both SSP2-4.5 and SSP5-8.5 (at the
310 99% confidence level), indicating that climate warming predominantly amplifies the mean
311 frequency of hot-related extremes rather than their temporal variability. For cold-related extremes,
312 CD exhibits more stronger changes than CW, which are also predominantly driven by reduction in
313 Mn. Under SSP5-8.5, Mn for most CCEs increases significantly across nearly the entire basin, while
314 under SSP2-4.5, it remains relatively stable. In contrast, Var exhibits only minimal changes under
315 both scenarios.

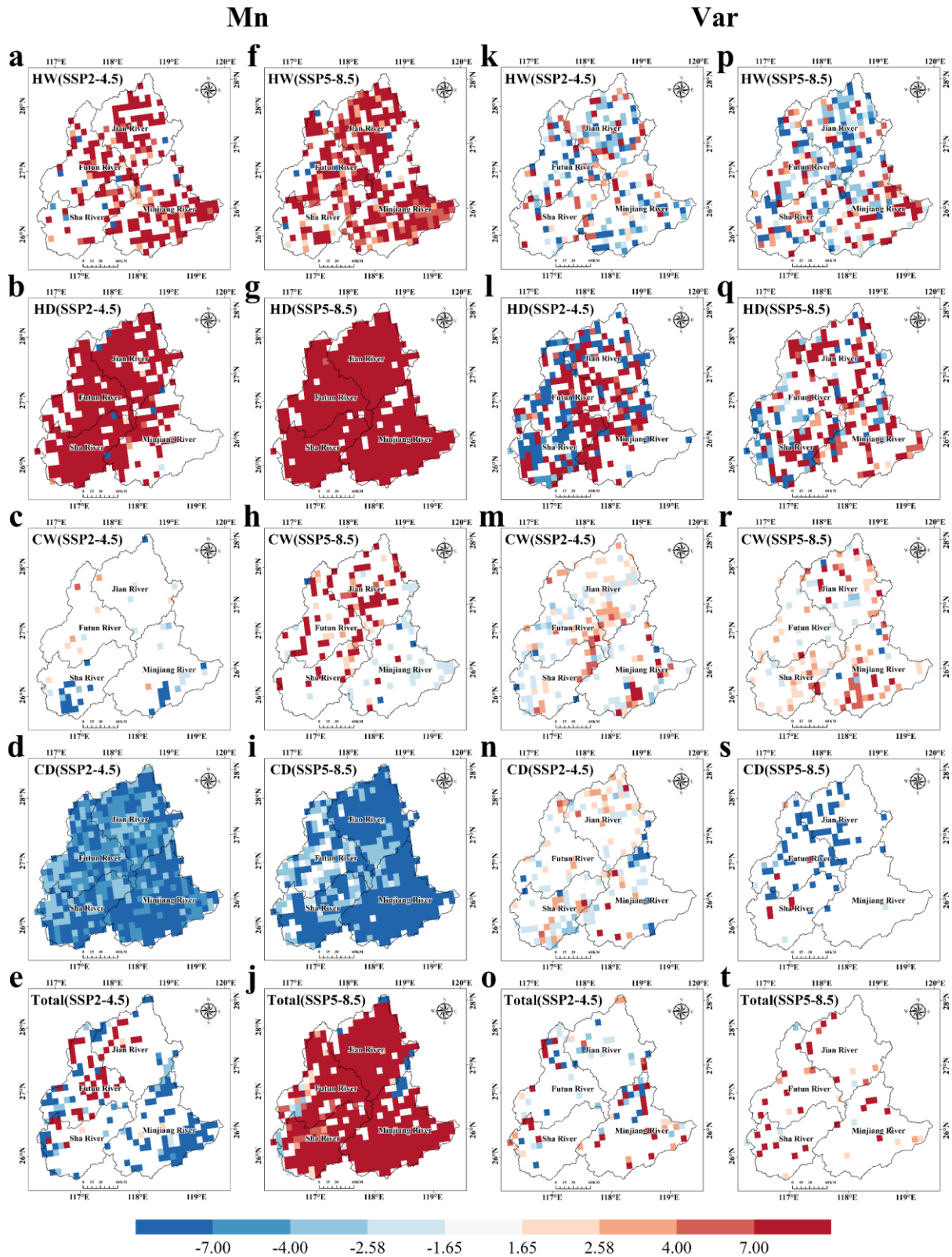


316

317 Figure 6. Stationary and non-stationary characteristics for CCEs in the MRB (a-e and k-o),

318 percentage of non-stationary and stationary characteristics across five basins (f-j and p-t).

319



320

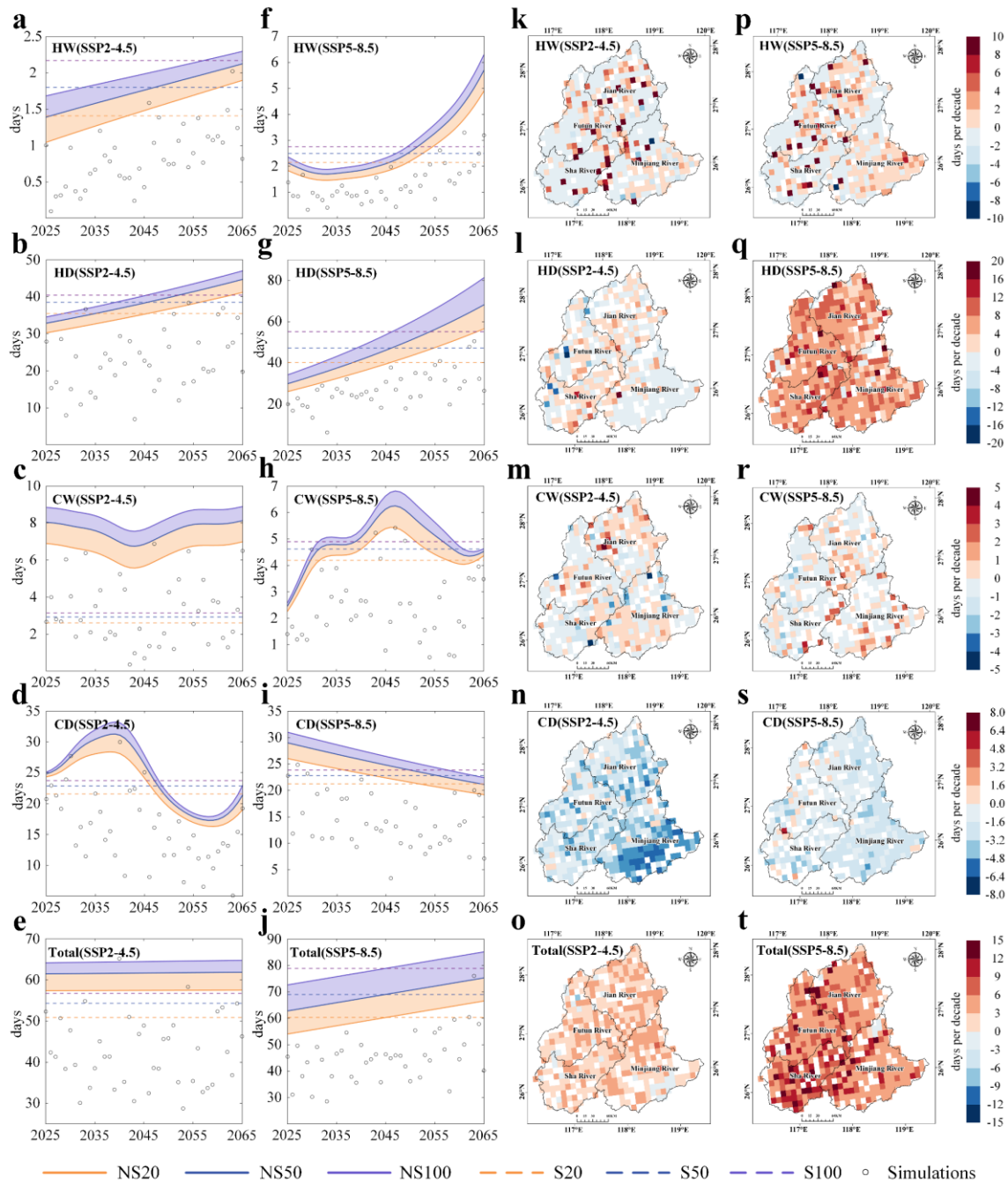
321 Figure 7. Results of Mann-Kendall test for Mn (a-j) and Var (k-t), showing the spatial distribution
 322 of Z values. Z values indicate trend significance: $|Z| > 1.65$ denotes 90% confidence, while $|Z| >$
 323 2.58 corresponds to 99% confidence.

324 **3.3 Changes in the recurrence frequency of CCEs**

325 To assess changes in the recurrence frequency of CCEs, we fit both stationary and non-
326 stationary models. As shown in Figures 8 (a-j), substantial differences emerge between the return
327 periods estimated under stationary versus non-stationary assumptions. Our results reveal that
328 stationary models systematically underestimate the future recurrence frequency of CCEs, whereas
329 non-stationary models reasonably capture their time-evolving characteristics. This underestimation
330 gap widens notably over time.

331 Under SSP5-8.5, non-stationary projections indicate significant increases in the frequency of
332 CCEs corresponding to 20-, 50-, and 100-year return periods. For instance, total CCEs with a 100-
333 year return period are projected to increase at a rate of 3.12 days per decade. Stationary models
334 consistently underestimate CEE frequency after around 2045. Specifically, HW, HD, and CW all
335 show positive trends in recurrence frequency under SSP5-8.5 with increases of 0.36, 11.65, and
336 0.30 days per decade, respectively. Under SSP2-4.5, the corresponding increases are lower
337 (0.15, 2.53, and 0.06 days per decade). In contrast, CD exhibits a decreasing trend, with a more
338 rapid decline under the SSP2-4.5 (-3.38 days per decade) than under SSP5-8.5. The 100-year return
339 events display greater sensitivity to climate change, highlighting amplified non-stationary effects
340 on these high-impact extremes.

341 We further quantify the deterministic trends in recurrence frequency using Empirical Mode
342 Decomposition (EMD, Supplement Method S1). Figures 8 k-t present the variations in the 100-year
343 recurrence frequency (complete results for all return periods are provided in Supplementary
344 Figure S7). Overall, CCE frequency shows strong upward trends under SSP5-8.5, with significant
345 spatial heterogeneity. Frequency generally decreases from west to east, with notably high-value
346 areas concentrated in the Shaxi River Basin (exceeding 12 days per decade in some grids). Among
347 all indices, HD exhibits the most severe increase, with basin-wide trends exceeding 8 days per
348 decade. CD is the only index showing a decreasing trend under both scenarios, with a less
349 pronounced decline under SSP5-8.5, suggesting that greenhouse warming has only partially offset
350 the reduction in CD recurrence frequency.



352

353 Figure 8. Comparison of non-stationary (NS) and stationary (S) characteristics for CCEs under 20-,
 354 50-, and 100- year return periods (a-j). Spatial distributions of trends in CCEs under 100-year return
 355 periods (k-t), 20- and 50-year return period result are provided in Supplement Figure S7. Blank
 356 areas indicate grid points that failed to pass the 99% confidence test.

357 **4 Discussion**

358 Although earlier research has emphasized the necessity of analyzing extreme events under
359 non-stationary conditions (Cheng et al, 2014; Byun and Hamlet, 2020; Liu et al., 2024), the
360 evolution of CCEs within a non-stationary climate remains lacking. Our study develops an
361 innovative non-stationary framework integrating WRF-based dynamical downscaling with
362 GAMLSS to reassess future recurrence frequency of CCEs. The results indicate that traditional
363 stationary models systematically underestimate the frequency of CCEs, highlighting the critical
364 importance of incorporating time-varying risk assessments to avoid misleading projections and to
365 inform robust climate adaptation strategies (Abdelmoaty and Papalexiou, 2023). This innovative
366 framework enables regional-scale reassessment of CCEs which is transferable to other regions.

367 **4.1 Dominance of hot extremes and temperature-driven shifts**

368 The projected increase in CCEs, particularly under SSP5-8.5, aligns with global trends of
369 intensifying hydroclimatic risks under continued warming (Asadieh and Krakauer, 2017; Zhang et
370 al., 2021; Shu et al., 2024). Our findings indicate that hot-dry extremes dominate both spatially and
371 temporally, increasing at 2.26 days per decade in summer under SSP5-8.5, while cold extremes
372 decline. This pattern is consistent with studies highlighting the rising prevalence of hot-stagnation
373 and hot-dry extremes in East Asia (Yin et al., 2025). In particular, across China, hot–dry extremes
374 are projected to double by 2050 under high-emission scenarios (Yao et al., 2024). Guo et al. (2023)
375 also revealed that under global warming, extreme hot conditions are projected to dominate most
376 regions of China, with some areas experiencing more than 50 extreme hot days. Moreover, there is
377 evidence suggesting that both compound hot–dry and compound hot–wet events are projected to
378 increase significantly under future climate scenarios. Notably, compound hot–dry events exhibit
379 substantially higher frequency, longer duration, and greater intensity than compound hot–wet
380 events (Fang et al., 2025). The reversal between hot and cold extremes has been robustly linked to
381 enhanced radiative forcing from anthropogenic greenhouse gas emissions (Samset et al., 2018;
382 Kramer et al., 2021). Our analysis further reveals that temperature—not precipitation—is the
383 primary driver of CCE changes in the MRB, as evidenced by the strong warming trend (0.46°C per
384 decade under SSP5-8.5) alongside relatively stable precipitation (Supplement Figure S5). This
385 supports the hypothesis that thermodynamic effects, rather than dynamic ones, dominate mean-state

386 changes in extremes (Horton et al., 2016; Van Der Wiel and Bintanja, 2021). However, it should be
387 emphasized that precipitation responses are often manifested through pronounced changes in
388 intensity and intermittency, rather than in long-term totals alone (Du et al., 2022; Maity and Maity,
389 2022). In particular, warming can lead to a redistribution of precipitation toward shorter duration
390 but more intense events, even in regions where mean precipitation exhibits statistically insignificant
391 trends (Fowler et al., 2021). For HW events, these changes are closely linked to both
392 thermodynamic and moisture-related processes. As global and regional temperatures rise, the
393 atmosphere’s moisture holding capacity increases at an approximate rate of 6–7% per °C, consistent
394 with Clausius–Clapeyron scaling (O’Gorman and Muller, 2010; Ali et al., 2021). Previous studies
395 have demonstrated that such moistening effects can substantially intensify CCEs, even in regions
396 where average precipitation remains relatively unchanged (Gimeno et al., 2022; Zhang et al., 2024).

397 **4.2 Non-stationarity: mean shifts outpace variability**

398 A key advance of this study is the explicit detection of non-stationary characteristics in CCEs,
399 which has been largely overlooked in prior compound event analyses. We find that under SSP5-8.5,
400 95.20% of grid cells exhibit non-stationarity, predominantly driven by changes in the Mn rather
401 than Var, accounting for 80.81% of the transitions. This suggests that climate warming amplifies
402 extremes primarily through shifts in baseline intensity—a thermodynamic effect—rather than
403 through increased temporal variability. Similar findings have been reported at global scales, where
404 mean warming dominates changes in extreme temperature distributions (Patel et al., 2024; Nordling
405 et al., 2025). The spatial concentration of Mn-driven non-stationarity in downstream MRB and the
406 Shaxi River Basin may reflect localized warming amplification due to urban heat islands or land-
407 atmosphere feedbacks, a phenomenon noted in other subtropical regions (Gao et al., 2018; Wu et
408 al., 2020).

409 **4.3 Frequency of recurrence systematically underestimated by stationary model**

410 Our comparison between stationary and non-stationary model indicates that the latter captures
411 a significant increase in recurrence risks, particularly for 100-year CCEs, which are projected to
412 rise by 3.12 days per decade under the SSP5-8.5 scenario. Stationary model systematically
413 underestimates recurrence frequency after 2045, and the stronger non-stationary response of 100-
414 year events highlights the heightened vulnerability of high-impact, low-probability extremes.

415 Additionally, the west-to-east gradient in recurrence frequency, with hotspots in the Shaxi River
416 Basin, may be attributed to topographic and land-surface heterogeneity, which modulate local
417 hydroclimatic responses (Zheng et al., 2023). The projected increase in the frequency of 100-year
418 CCEs has important implications for flood control and water resources management in the MRB,
419 particularly in the middle and lower reaches and densely populated urban centers such as Fuzhou.
420 The basin's complex topography and highly heterogeneous land cover amplify the spatial
421 variability of rainfall and runoff, while low-lying urban areas in Fuzhou are particularly vulnerable
422 to both pluvial and fluvial flooding. More frequent HW events are likely to produce intense,
423 concentrated rainfall, rapidly depleting reservoir flood control capacity and increasing the
424 likelihood of spillway activation, while simultaneously exacerbating urban inundation in flood
425 prone districts (He et al., 2024). HD events may reduce river storage, but if followed by subsequent
426 heavy rainfall, they can increase uncertainty in peak flows and place additional stress on flood
427 management systems (Hariharan Sudha et al., 2024). Previous studies have similarly shown that
428 conventional extreme value models fail to capture the escalating severity of extreme events under
429 climate change. Singh et al. (2021) demonstrated that under climate change, precipitation and
430 temperature exhibit a non-stationary dependent structure, and treating them independently can
431 substantially underestimate the occurrence of compound extremes. Feng et al. (2020) compared the
432 recurrence probabilities of floods under stationary and non-stationary conditions and found that,
433 under non-stationary conditions, the annual variability of floods is significantly greater. Xu et al.
434 (2025) evaluated changes in global marine heatwaves and found that stationary models significantly
435 underestimate their frequency, intensity, and duration. In summary, these studies collectively
436 highlight that accounting for non-stationarity is crucial for accurately assessing various extreme
437 events.

438 **4.4 Methodological limitations**

439 Our integrated 'bias-corrected CMIP6–WRF dynamical downscaling–GAMLSS' framework
440 represents a significant methodological advancement over the direct use of purely statistical
441 downscaling for projecting CCEs. By resolving mesoscale circulations and explicitly simulating
442 convective processes, our approach more faithfully captures the fine-scale spatiotemporal
443 heterogeneity of precipitation and temperature fields in complex terrain, a capability that statistical

444 methods, reliant on historically derived statistical relationships, fundamentally lack (Gutmann et
445 al., 2012; Rahimi et al., 2024). Nevertheless, certain limitations persist. Even at convection-
446 permitting resolution (3 km), the WRF model exhibits systematic biases in simulating orographic
447 precipitation, a well-documented challenge often stemming from uncertainties in microphysical
448 parameterization schemes and the representation of land-atmosphere energy and moisture
449 exchanges over mountainous regions (Talbot et al., 2012; Zhang et al., 2025). Specifically, the
450 overestimation of precipitation in high-elevation regions by WRF may artificially enhance the
451 frequency of wet-related compound extremes, whereas the underestimation of precipitation in
452 lowland and downstream areas may bias the detection of dry-related compound extremes. Because
453 the identification of CCEs relies on precipitation and temperature thresholds and their co-
454 occurrence, systematic precipitation biases can further influence threshold estimation and event
455 classification, thereby affecting the spatial distribution and frequency of detected CCEs. To address
456 this limitation in future work, we plan to explore machine learning based post-processing
457 approaches (Yin et al., 2021; Xie et al., 2023), in which the residuals between historical WRF
458 simulations and station observations are learned and subsequently transferred to future simulations
459 in a physically constrained method. This approach offers a promising pathway to reduce systematic
460 regional model biases while preserving the internally consistent climate change signal. Furthermore,
461 while statistically robust, our current non-stationary GAMLSS framework employs time merely as
462 a proxy covariate for climate change. While this formulation is widely adopted and effective for
463 detecting long-term trends, time itself serves only as an indirect proxy for the underlying physical
464 processes driving changes in CCEs (Ragno et al., 2019). From a physical perspective, the evolution
465 of compound hot–dry events are governed by a combination of thermodynamic and dynamic
466 mechanisms, including background warming, shifts in large-scale atmospheric circulation, and
467 land–atmosphere feedbacks (Bevacqua et al., 2022; Zhang et al., 2021; Tian et al., 2024). For
468 example, global mean surface temperature (GMST) can serve as a physically meaningful indicator
469 of anthropogenic thermodynamic forcing, directly linking greenhouse gas increases to enhanced
470 surface heat stress (Gillett et al., 2021). In this subtropical monsoon dominated basin, variations in
471 the intensity, westward extension, and persistence of the Western Pacific Subtropical High (WPSH)
472 can regulate subsidence strength, cloud cover, and surface radiative forcing, thereby favoring

473 persistent hot conditions while suppressing precipitation (Li et al., 2024; An et al., 2025). Changes
474 in the strength and variability of the East Asian summer monsoon (EASM) influence large-scale
475 moisture transport and rainfall timing, affecting both the onset and persistence of dry spells (Park
476 et al., 2020; Dou et al., 2025). In addition, antecedent soil moisture has been shown to influence the
477 persistence and amplification of heat extremes through soil moisture–temperature feedbacks (Jiang
478 and Wang, 2024), further highlighting the value of including land-surface states as covariates.
479 Therefore, incorporating physically based covariates into the GAMLSS framework may therefore
480 improve the interpretation of non-stationarity.

481 **5 Conclusions**

482 Through this intensive case analysis, we establish a transferable framework for assessing the
483 non-stationarity of CCEs. This work advances the understanding of the evolution of CCE
484 recurrence frequency under climate change and offers important perspectives to support adaptive
485 strategies and strengthen disaster risk governance. The main findings are summarized as follows:

486 1) CCEs increase significantly across the MRB, with a stronger trend under SSP5-8.5 (3.55 days
487 per decade) than under SSP2-4.5. HD extremes dominate both spatially (downstream-focused)
488 and seasonally (summer-peaked), rising at 2.26 days per decade, whereas cold extremes decline.
489 These shifts are primarily temperature-driven, as pronounced warming amplifies hot-related
490 extremes but suppresses cold-related extremes.

491 2) CCEs shift markedly toward Mn-dominated non-stationarity under SSP5-8.5 scenarios,
492 contrasting with the largely stationarity under SSP2-4.5. Spatially, Mn non-stationarity governs
493 80.8 % of the MRB under SSP5-8.5, with dry-related extremes (HD and CD) showing the most
494 abrupt transitions. For HD, Mn non-stationarity expands from 22.7% to 57.0% of the basin and
495 dominates 60% of downstream grids—an increase of nearly threefold relative to SSP2-4.5. For
496 CD, Mn-driven shifts cover >90% of the downstream MRB. Var contributes minimally in both
497 scenarios, confirming that warming amplifies extremes primarily through shifts in mean intensity
498 rather than through increased variability.

499 3) Non-stationary modeling reveals that stationary approaches systematically underestimate future
500 CCEs recurrence frequency. Under SSP5-8.5, most CCEs types (except CD) exhibit increasing
501 recurrence frequency. Climate change impacts are significantly amplified for 100-year return

502 period events, which rise at 3.12 days per decade—a response highlighting their heightened
503 non-stationary sensitivity. Spatially, recurrence frequency shows a distinct east-to-west gradient,
504 with a significantly increase occurring in the western mountainous areas.

505 **Acknowledgements**

506 The ‘High Performance Computing Center’ at Fujian Normal University provided
507 computational resources for the WRF model simulations.

508 **Financial support**

509 Supported by the National Natural Science Foundation of China (Grant No. 42271030), the
510 Scientific Project of Fujian Provincial Department of Science and Technology (Grant no.
511 2022Y0007), the German Federal Ministry of Education and Research (BMBF) through funding of
512 the KARE_II project (01LR2006D1) and the ‘Young Eagle Plan’ Top Talents of Fujian Province.
513 Lu Gao is financially supported by the Humboldt Research Fellowship for Experienced Researchers
514 through Alexander von Humboldt Foundation. Yinchu Zhang gratefully acknowledge financial
515 support from the China Scholarship Council (CSC).

516 **Code/Data availability**

517 Code/Data will be made available on request.

518 **Declaration of competing interest**

519 The authors declare that they have no known competing financial interests or personal
520 relationships that could have appeared to influence the work reported in this paper.

521 **Author contribution**

522 Conceptualization: YZ. Methodology: YZ, LG, WX, CD, MM, JW, HK. Software: YZ, WX,
523 CD. Data curation: SS. Writing- Original draft preparation: YZ. Writing- Reviewing and Editing:
524 WX, YW, LG. Supervision: SS, MM, YC, HK. Funding acquisition: LG, JW, YC.

525 **References**

- 526 Abdelmoaty, H. M. and Papalexiou, S. M.: Changes of Extreme Precipitation in CMIP6 Projections:
527 Should We Use Stationary or Nonstationary Models, *J. Climate*, 36, 2999–3014,
528 <https://doi.org/10.1175/JCLI-D-22-0467.1>, 2023.
- 529 Ali, H., Fowler, H. J., Lenderink, G., Lewis, E., and Pritchard, D.: Consistent Large - Scale
530 Response of Hourly Extreme Precipitation to Temperature Variation Over Land, *Geophys. Res.*
531 *Lett.*, 48, e2020GL090317, <https://doi.org/10.1029/2020GL090317>, 2021.
- 532 An, X., Sun, S., Ma, Q., Wu, H., Li, D., and Wu, W.: Elucidating the Varied Characteristics of
533 Compound Hot–Drought from Two Distinctive Extreme Events in the Yangtze River Valley,
534 *Int. J. Climatol.*, 45, e8809, <https://doi.org/10.1002/joc.8809>, 2025. Arakawa, A. and Jung, J.-
535 H.: Multiscale modeling of the moist-convective atmosphere — A review, *Atmos. Res.*, 102,
536 263–285, <https://doi.org/10.1016/j.atmosres.2011.08.009>, 2011.
- 537 Arnault, J., Jung, G., Haese, B., Fersch, B., Rummler, T., Wei, J., Zhang, Z., and Kunstmann, H.: A
538 Joint Soil - Vegetation - Atmospheric Modeling Procedure of Water Isotopologues:
539 Implementation and Application to Different Climate Zones With WRF - Hydro - Iso, *J. Adv.*
540 *Model Earth Syst.*, 13, <https://doi.org/10.1029/2021MS002562>, 2021.
- 541 Asadieh, B. and Krakauer, N. Y.: Global change in streamflow extremes under climate change over
542 the 21st century, *Hydrol. Earth Syst. Sci.*, 21, 5863–5874, [https://doi.org/10.5194/hess-21-](https://doi.org/10.5194/hess-21-5863-2017)
543 [5863-2017](https://doi.org/10.5194/hess-21-5863-2017), 2017.
- 544 Bevacqua, E., Zappa, G., Lehner, F., and Zscheischler, J.: Precipitation trends determine future
545 occurrences of compound hot–dry events, *Nat. Clim. Chang.*, 12, 350–355,
546 <https://doi.org/10.1038/s41558-022-01309-5>, 2022.
- 547 Byun, K. and Hamlet, A. F.: A risk-based analytical framework for quantifying non-stationary flood
548 risks and establishing infrastructure design standards in a changing environment, *J. Hydrol.*,
549 584, 124575, <https://doi.org/10.1016/j.jhydrol.2020.124575>, 2020.
- 550 Byun, U., Chang, E., Kim, J., Ahn, J., Cha, D., Min, S., and Byun, Y.: Investigation of Added Value
551 in Regional Climate Models for East Asian Storm Track Analysis, *J. Geophys. Res.: Atmos.*,
552 128, e2023JD039167, <https://doi.org/10.1029/2023JD039167>, 2023.

553 Chen, G., Mei, S.-J., Hang, J., Li, Q., and Wang, X.: URANS simulations of urban microclimates:
554 Validated by scaled outdoor experiments, *Building and Environment*, 272, 112691,
555 <https://doi.org/10.1016/j.buildenv.2025.112691>, 2025.

556 Chen, S.-H. and Sun, W.-Y.: A One-dimensional Time Dependent Cloud Model, *J. Meteorol. Soc.*
557 *Japan.*, 80, 99–118, <https://doi.org/10.2151/jmsj.80.99>, 2002.

558 Cheng, L., AghaKouchak, A., Gilleland, E., and Katz, R. W.: Non-stationary extreme value analysis
559 in a changing climate, *Climatic Change*, 127, 353–369, [https://doi.org/10.1007/s10584-014-](https://doi.org/10.1007/s10584-014-1254-5)
560 1254-5, 2014.

561 Croitoru, A.-E., Piticar, A., Ciupertea, A.-F., and Roșca, C. F.: Changes in heat waves indices in
562 Romania over the period 1961–2015, *Global and Planetary Change*, 146, 109–121,
563 <https://doi.org/10.1016/j.gloplacha.2016.08.016>, 2016.

564 Dou, Z., Liu, B., Henderson, M., Zhou, W., Ma, R., Chen, M., and Zhang, Z.: Changes in Timing
565 and Precipitation of the East Asian Summer Monsoon over China Between 1960 and 2017,
566 *Earth*, 6, 24, <https://doi.org/10.3390/earth6020024>, 2025.

567 Du, H., Donat, M. G., Zong, S., Alexander, L. V., Manzanas, R., Kruger, A., Choi, G., Salinger, J.,
568 He, H. S., Li, M.-H., Fujibe, F., Nandintsetseg, B., Rehman, S., Abbas, F., Rusticucci, M.,
569 Srivastava, A., Zhai, P., Lippmann, T., Yabi, I., Stambaugh, M. C., Wang, S., Batbold, A.,
570 Oliveira, P. T. D., Adrees, M., Hou, W., Silva, C. M. S. E., Lucio, P. S., and Wu, Z.: Extreme
571 Precipitation on Consecutive Days Occurs More Often in a Warming Climate, *B. Am.*
572 *Meteorol. Soc.*, 103, E1130–E1145, <https://doi.org/10.1175/BAMS-D-21-0140.1>, 2022.

573 Duan, R., Huang, G., Wang, F., Tian, C., and Wu, X.: Observations Over a Century Underscore an
574 Increasing Likelihood of Compound Dry - Hot Events in China, *Earth ’ s Future*, 12,
575 e2024EF004546, <https://doi.org/10.1029/2024EF004546>, 2024.

576 Dudhia, J.: Numerical Study of Convection Observed during the Winter Monsoon Experiment
577 Using a Mesoscale Two-Dimensional Model, *J. Atmos. Sci.*, 46, 3077–3107,
578 [https://doi.org/10.1175/1520-0469\(1989\)046%253C3077:NSOCOD%253E2.0.CO;2](https://doi.org/10.1175/1520-0469(1989)046%253C3077:NSOCOD%253E2.0.CO;2), 1989.

579 Fang, P., Wang, T., Yang, D., Tang, L., and Yang, Y.: Substantial increases in compound climate
580 extremes and associated socio-economic exposure across China under future climate change,
581 *npj Clim. Atmos Sci.*, 8, 17, <https://doi.org/10.1038/s41612-025-00910-7>, 2025.

582 Feng, Y., Shi, P., Qu, S., Mou, S., Chen, C., and Dong, F.: Nonstationary flood coincidence risk
583 analysis using time-varying copula functions, *Sci. Rep.*, 10, 3395,
584 <https://doi.org/10.1038/s41598-020-60264-3>, 2020.

585 Filliben, J. J.: The Probability Plot Correlation Coefficient Test for Normality, *Technometrics*, 17,
586 111–117, <https://doi.org/10.1080/00401706.1975.10489279>, 1975.

587 Fowler, H. J., Lenderink, G., Prein, A. F., Westra, S., Allan, R. P., Ban, N., Barbero, R., Berg, P.,
588 Blenkinsop, S., Do, H. X., Guerreiro, S., Haerter, J. O., Kendon, E. J., Lewis, E., Schaer, C.,
589 Sharma, A., Villarini, G., Wasko, C., and Zhang, X.: Anthropogenic intensification of short-
590 duration rainfall extremes, *Nat. Rev. Earth Environ.*, 2, 107–122,
591 <https://doi.org/10.1038/s43017-020-00128-6>, 2021.

592 Gan, B., Liu, M., Cui, H., Chen, X., Chen, Y., Gao, L., and Deng, H.: Spatiotemporal patterns and
593 propagation of meteorological and hydrological drought in a humid basin of Southeast China,
594 *Sci. Rep.*, 15, 31720, <https://doi.org/10.1038/s41598-025-17005-1>, 2025.

595 Gao, L., Huang, J., Chen, X., Chen, Y., and Liu, M.: Contributions of natural climate changes and
596 human activities to the trend of extreme precipitation, *Atmos. Res.*, 205, 60–69,
597 <https://doi.org/10.1016/j.atmosres.2018.02.006>, 2018.

598 Geng, K., Chen, X., Zheng, M., Gao, Y., Gu, Z., and Yao, H.: The influence of human activities on
599 rainfall-runoff relationships at different time scales in the Minjiang River Basin, *Theor. Appl.*
600 *Climatol.*, 155, 8435–8454, <https://doi.org/10.1007/s00704-024-05124-0>, 2024.

601 Gilbert, E., Pishniak, D., Torres, J. A., Orr, A., Maclennan, M., Wever, N., and Verro, K.: Extreme
602 precipitation associated with atmospheric rivers over West Antarctic ice shelves: insights from
603 kilometre-scale regional climate modelling, *The Cryosphere*, 19, 597–618,
604 <https://doi.org/10.5194/tc-19-597-2025>, 2025.

605 Gillett, N. P., Kirchmeier-Young, M., Ribes, A., Shiogama, H., Hegerl, G. C., Knutti, R., Gastineau,
606 G., John, J. G., Li, L., Nazarenko, L., Rosenbloom, N., Seland, Ø., Wu, T., Yukimoto, S., and
607 Ziehn, T.: Constraining human contributions to observed warming since the pre-industrial
608 period, *Nat. Clim. Chang.*, 11, 207–212, <https://doi.org/10.1038/s41558-020-00965-9>, 2021.

609 Gimeno, L., Sorí, R., Vázquez, M., Stojanovic, M., Algarra, I., Eiras - Barca, J., Gimeno - Sotelo,
610 L., and Nieto, R.: Extreme precipitation events, *WIREs Water*, 9, e1611,
611 <https://doi.org/10.1002/wat2.1611>, 2022.

612 Guo, J., Wang, X., Fan, Y., Liang, X., Jia, H., and Liu, L.: How Extreme Events in China Would Be
613 Affected by Global Warming—Insights From a Bias - Corrected CMIP6 Ensemble, *Earth’ s*
614 *Future*, 11, e2022EF003347, <https://doi.org/10.1029/2022EF003347>, 2023.

615 Gutmann, E. D., Rasmussen, R. M., Liu, C., Ikeda, K., Gochis, D. J., Clark, M. P., Dudhia, J., and
616 Thompson, G.: A Comparison of Statistical and Dynamical Downscaling of Winter
617 Precipitation over Complex Terrain, *J. Climate*, 25, 262–281,
618 <https://doi.org/10.1175/2011JCLI4109.1>, 2012.

619 Hariharan Sudha, S., Ragno, E., Morales-Nápoles, O., and Kok, M.: Investigating meteorological
620 wet and dry transitions in the Dutch Meuse River basin, *Front. Water*, 6, 1394563,
621 <https://doi.org/10.3389/frwa.2024.1394563>, 2024.

622 He, K., Chen, X., Zhou, J., Zhao, D., and Yu, X.: Compound successive dry-hot and wet extremes
623 in China with global warming and urbanization, *J. Hydrol.*, 636, 131332,
624 <https://doi.org/10.1016/j.jhydrol.2024.131332>, 2024.

625 Hong, S.-Y., Noh, Y., and Dudhia, J.: A New Vertical Diffusion Package with an Explicit Treatment
626 of Entrainment Processes, *Mon. Weather Rev.*, 134, 2318–2341,
627 <https://doi.org/10.1175/MWR3199.1>, 2006.

628 Horton, R. M., Mankin, J. S., Lesk, C., Coffel, E., and Raymond, C.: A Review of Recent Advances
629 in Research on Extreme Heat Events, *Curr. Clim. Change Rep.*, 2, 242–259,
630 <https://doi.org/10.1007/s40641-016-0042-x>, 2016.

631 Huang, N. E., Shen, Z., Long, S. R., Wu, M. C., Shih, H. H., Zheng, Q., Yen, N.-C., Tung, C. C.,
632 and Liu, H. H.: The empirical mode decomposition and the Hilbert spectrum for nonlinear and
633 non-stationary time series analysis, *Proc. R. Soc. Lond. A*, 454, 903–995,
634 <https://doi.org/10.1098/rspa.1998.0193>, 1998.

635 Huang, Y., Xue, M., Hu, X., Martin, E., Novoa, H. M., McPherson, R. A., Liu, C., Chen, M., Hong,
636 Y., Perez, A., Morales, I. Y., Ticona Jara, J. L., and Flores Luna, A. J.: Increasing frequency
637 and precipitation intensity of convective storms in the Peruvian Central Andes: Projections

638 from convection - permitting regional climate simulations, *Quart. J. Royal Meteor. Soc.*, 150,
639 4371 - 4390, <https://doi.org/10.1002/qj.4820>, 2024.

640 Imran, H. M. and Evans, J. P.: Observational uncertainty in the added value of regional climate
641 modelling over Australia, *Clim. Dyn.*, 63, 73, <https://doi.org/10.1007/s00382-024-07562-y>,
642 2025.

643 IPCC.: Weather and climate extreme events in a changing climate. In *climate change: The physical*
644 *science basis. Contribution of Working Group I to the Sixth Assessment Report of the*
645 *Intergovernmental Panel on Climate Change. Cambridge University Press, Cambridge, United*
646 *Kingdom and New York, NY, USA, pp. 1513–1766, [https://doi: 10.1017/9781009157896.013](https://doi:10.1017/9781009157896.013),*
647 *2021.*

648 Jamal, K., Li, X., Chen, Y., Rizwan, M., Khan, M. A., Syed, Z., and Mahmood, P.: Bias correction
649 and projection of temperature over the altitudes of the Upper Indus Basin under CMIP6 climate
650 scenarios from 1985 to 2100, *J. Water Clim. Change*, 14, 2490–2514,
651 <https://doi.org/10.2166/wcc.2023.180>, 2023.

652 Jia, N., Cheng, J., Li, Y., Zheng, L., Song, W., Chen, R., and Zhu, A.: China's Yangtze River drought:
653 A cascade of impacts from mountains to sea, *Sci. China Earth Sci.*, 68, 957–962,
654 <https://doi.org/10.1007/s11430-024-1521-3>, 2025.

655 Jiang, Q., Li, W., Fan, Z., He, X., Sun, W., Chen, S., Wen, J., Gao, J., and Wang, J.: Evaluation of
656 the ERA5 reanalysis precipitation dataset over Chinese Mainland, *Journal of Hydrology*, 595,
657 125660, <https://doi.org/10.1016/j.jhydrol.2020.125660>, 2021.

658 Jiang, Y. and Wang, G.: Soil Moisture Dominates the Land Surface Feedback in the Development
659 of Compound Drought–Heat Extremes in Tropical South America, *J. Hydrometeorol.*, 25,
660 1649–1664, <https://doi.org/10.1175/JHM-D-24-0005.1>, 2024.

661 Kramer, R. J., He, H., Soden, B. J., Oreopoulos, L., Myhre, G., Forster, P. M., and Smith, C. J.:
662 Observational Evidence of Increasing Global Radiative Forcing, *Geophys. Res. Lett.*, 48,
663 e2020GL091585, <https://doi.org/10.1029/2020GL091585>, 2021.

664 Lee, T. and Ouarda, T. B. M. J.: Long - term prediction of precipitation and hydrologic extremes
665 with nonstationary oscillation processes, *J. Geophys. Res.*, 115, 2009JD012801,
666 <https://doi.org/10.1029/2009JD012801>, 2010.

667 Lei, X., Gao, L., Ma, M., Wei, J., Xu, L., Wang, L., and Lin, H.: Does non-stationarity of extreme
668 precipitation exist in the Poyang Lake Basin of China, *J. Hydrol.: Reg. Stud.*, 37, 100920,
669 <https://doi.org/10.1016/j.ejrh.2021.100920>, 2021.

670 Li, Z., Ren, H.-L., Lu, M., and Zhou, F.: Interannual variations of westward extension area of
671 western Pacific subtropical high and its relationship with precipitation in East Asia, *Atmos.*
672 *Res.*, 298, 107148, <https://doi.org/10.1016/j.atmosres.2023.107148>, 2024.

673 Lin, C., Kjellström, E., Wilcke, R. A. I., and Chen, D.: Present and future European heat wave
674 magnitudes: climatologies, trends, and their associated uncertainties in GCM-RCM model
675 chains, *Earth Syst. Dynam.*, 13, 1197–1214, <https://doi.org/10.5194/esd-13-1197-2022>, 2022.

676 Liu, H., Xiao, P., Zhang, X., Liang, Y., Tang, B., Chen, S., and Liu, Y.: Winter snowpack loss
677 increases warm-season compound hot-dry extremes, *Commun. Earth Environ.*, 5, 567,
678 <https://doi.org/10.1038/s43247-024-01734-8>, 2024a.

679 Lin, S., Zhang, Y., Sun, S., Guan, X., Jiang, C., Gao, L.: Sensitivity study of WRF parameterization
680 schemes and initial fields on simulation of rainstorm in the Minjiang River basin. *Pearl River*
681 *(in Chinese)* 44(10):35-46+61. [https://doi: 10.3969/j.issn.1001-9235.2023.10.004](https://doi:10.3969/j.issn.1001-9235.2023.10.004), 2023.

682 Liu, Y., Chen, J., Xiong, L., and Xu, C.-Y.: Integrating heterogeneous information for modeling
683 non-stationarity of extreme precipitation in the Yangtze River Basin, *J. Hydrol.*, 645, 132159,
684 <https://doi.org/10.1016/j.jhydrol.2024.132159>, 2024b.

685 Ma, L., Hu, S., Zhou, B., Peng, J., and Li, D.: Novel dynamical indices for the variations of the
686 South Asia high in a warming climate, *Atmos. Res.*, 315, 107901,
687 <https://doi.org/10.1016/j.atmosres.2024.107901>, 2025.

688 Maity, S. S. and Maity, R.: Changing Pattern of Intensity–Duration–Frequency Relationship of
689 Precipitation due to Climate Change, *Water Resour. Manage.*, 36, 5371–5399,
690 <https://doi.org/10.1007/s11269-022-03313-y>, 2022.

691 Miao, L., Ju, L., Sun, S., Agathokleous, E., Wang, Q., Zhu, Z., Liu, R., Zou, Y., Lu, Y., and Liu, Q.:
692 Unveiling the dynamics of sequential extreme precipitation-heatwave compounds in China,
693 *npj Clim. Atmos. Sci.*, 7, 67, <https://doi.org/10.1038/s41612-024-00613-5>, 2024.

694 Min, Y., Huang, W., Ma, M., and Zhang, Y.: Simulations in the Topography Effects of Tianshan
695 Mountains on an Extreme Precipitation Event in the Ili River Valley, China, *Atmosphere*, 12,
696 750, <https://doi.org/10.3390/atmos12060750>, 2021.

697 Mlawer, E. J., Taubman, S. J., Brown, P. D., Iacono, M. J., and Clough, S. A.: Radiative transfer for
698 inhomogeneous atmospheres: RRTM, a validated correlated - k model for the longwave, *J.*
699 *Geophys. Res.*, 102, 16663 – 16682, <https://doi.org/10.1029/97JD00237>, 1997.

700 Mukherjee, S., Mishra, A. K., Zscheischler, J., and Entekhabi, D.: Interaction between dry and hot
701 extremes at a global scale using a cascade modeling framework, *Nat. Commun.*, 14, 277,
702 <https://doi.org/10.1038/s41467-022-35748-7>, 2023.

703 Nerantzaki, S. D., Papalexiou, S. M., Rajulapati, C. R., and Clark, M. P.: Nonstationarity in High
704 and Low - Temperature Extremes: Insights From a Global Observational Data Set by Merging
705 Extreme - Value Methods, *Earth's Future*, 11, e2023EF003506,
706 <https://doi.org/10.1029/2023EF003506>, 2023.

707 Niu, G.-Y., Yang, Z.-L., Mitchell, K. E., Chen, F., Ek, M. B., Barlage, M., Kumar, A., Manning, K.,
708 Niyogi, D., Rosero, E., Tewari, M., and Xia, Y.: The community Noah land surface model with
709 multiparameterization options (Noah-MP): 1. Model description and evaluation with local-
710 scale measurements, *J. Geophys. Res.*, 116, D12109, <https://doi.org/10.1029/2010JD015139>,
711 2011.

712 Nordling, K., Fahrenbach, N. L. S., and Samset, B. H.: Climate variability can outweigh the
713 influence of climate mean changes for extreme precipitation under global warming, *Atmos.*
714 *Chem. Phys.*, 25, 1659–1684, <https://doi.org/10.5194/acp-25-1659-2025>, 2025.

715 O’Gorman, P. A. and Muller, C. J.: How closely do changes in surface and column water vapor
716 follow Clausius–Clapeyron scaling in climate change simulations, *Environ. Res. Lett.*, 5,
717 025207, <https://doi.org/10.1088/1748-9326/5/2/025207>, 2010.

718 Park, J., Kim, H., Simon Wang, S.-Y., Jeong, J.-H., Lim, K.-S., LaPlante, M., and Yoon, J.-H.:
719 Intensification of the East Asian summer monsoon lifecycle based on observation and CMIP6,
720 *Environ. Res. Lett.*, 15, 0940b9, <https://doi.org/10.1088/1748-9326/ab9b3f>, 2020.

721 Patel, R. N., Bonan, D. B., and Schneider, T.: Changes in the Frequency of Observed Temperature
722 Extremes Largely Driven by a Distribution Shift, *Geophys. Res. Lett.*, 51, e2024GL110707,
723 <https://doi.org/10.1029/2024GL110707>, 2024.

724 Qian, C.: On trend estimation and significance testing for non-Gaussian and serially dependent data:
725 quantifying the urbanization effect on trends in hot extremes in the megacity of Shanghai,
726 *Clim. Dyn.*, 47, 329–344, <https://doi.org/10.1007/s00382-015-2838-0>, 2016.

727 Ragno, E., AghaKouchak, A., Cheng, L., and Sadegh, M.: A generalized framework for process-
728 informed nonstationary extreme value analysis, *Adv. Water Resour.*, 130, 270–282,
729 <https://doi.org/10.1016/j.advwatres.2019.06.007>, 2019.

730 Rahimi, S., Huang, L., Norris, J., Hall, A., Goldenson, N., Risser, M., Feldman, D. R., Lebo, Z. J.,
731 Dennis, E., and Thackeray, C.: Understanding the Cascade: Removing GCM Biases Improves
732 Dynamically Downscaled Climate Projections, *Geophys. Res. Lett.*, 51, e2023GL106264,
733 <https://doi.org/10.1029/2023GL106264>, 2024.

734 Ridder, N. N., Ukkola, A. M., Pitman, A. J., and Perkins-Kirkpatrick, S. E.: Increased occurrence
735 of high impact compound events under climate change, *npj Clim. Atmos. Sci.*, 5, 3,
736 <https://doi.org/10.1038/s41612-021-00224-4>, 2022.

737 Rigby, R. A. and Stasinopoulos, D. M.: Generalized Additive Models for Location, Scale and Shape,
738 *J. R. Stat. Soc. C-Appl.*, 54, 507–554, <https://doi.org/10.1111/j.1467-9876.2005.00510.x>, 2005.

739 Salarijazi, M., Ghorbani, K., Mohammadi, M., Ahmadianfar, I., Mohammadrezapour, O., Naser, M.
740 H., and Yaseen, Z. M.: Spatial-temporal estimation of maximum temperature high returns
741 periods for annual time series considering stationary/nonstationary approaches in Iran urban
742 area, *Urban Clim.*, 49, 101504, <https://doi.org/10.1016/j.uclim.2023.101504>, 2023.

743 Samset, B. H., Sand, M., Smith, C. J., Bauer, S. E., Forster, P. M., Fuglestedt, J. S., Osprey, S., and
744 Schleussner, C. - F.: Climate Impacts from a Removal of Anthropogenic Aerosol Emissions,
745 *Geophys. Res. Lett.*, 45, 1020 – 1029, <https://doi.org/10.1002/2017GL076079>, 2018.

746 Sauter, C., Fowler, H. J., Westra, S., Ali, H., Peleg, N., and White, C. J.: Compound extreme hourly
747 rainfall preconditioned by heatwaves most likely in the mid-latitudes, *Weather Clim. Extremes*,
748 40, 100563, <https://doi.org/10.1016/j.wace.2023.100563>, 2023.

749 Shang, S., Arnault, J., Zhu, G., Chen, H., Wei, J., Zhang, K., Zhang, Z., Laux, P., and Kunstmann,
750 H.: Recent Increase of Spring Precipitation over the Three-River Headwaters Region—Water
751 Budget Analysis Based on Global Reanalysis (ERA5) and ET-Tagging Extended Regional
752 Climate Modeling, *J. Climate*, 35, 7199–7217, <https://doi.org/10.1175/JCLI-D-21-0829.1>,
753 2022.

754 Shao, S., Zhang, H., Singh, V. P., Ding, H., Zhang, J., and Wu, Y.: Nonstationary analysis of
755 hydrological drought index in a coupled human-water system: Application of the GAMLSS
756 with meteorological and anthropogenic covariates in the Wuding River basin, China, *J. Hydrol.*,
757 608, 127692, <https://doi.org/10.1016/j.jhydrol.2022.127692>, 2022.

758 Shu, Z., Jin, J., Zhang, J., Wang, G., Lian, Y., Liu, Y., Bao, Z., Guan, T., He, R., Liu, C., and Jing,
759 P.: 1.5°C and 2.0°C of global warming intensifies the hydrological extremes in China, *J.*
760 *Hydrol.*, 635, 131229, <https://doi.org/10.1016/j.jhydrol.2024.131229>, 2024.

761 Singh, H., Najafi, M. R., and Cannon, A. J.: Characterizing non-stationary compound extreme
762 events in a changing climate based on large-ensemble climate simulations, *Clim. Dyn.*, 56,
763 1389–1405, <https://doi.org/10.1007/s00382-020-05538-2>, 2021.

764 Song, X., Zhang, J., Zou, X., Zhang, C., AghaKouchak, A., and Kong, F.: Changes in precipitation
765 extremes in the Beijing metropolitan area during 1960–2012, *Atmos. Res.*, 222, 134–153,
766 <https://doi.org/10.1016/j.atmosres.2019.02.006>, 2019.

767 Stasinopoulos, D. M. and Rigby, R. A.: Generalized Additive Models for Location Scale and Shape
768 (GAMLSS) in R, *J. Stat. Soft.*, 23, <https://doi.org/10.18637/jss.v023.i07>, 2007.

769 Sun, F., Roderick, M. L., and Farquhar, G. D.: Rainfall statistics, stationarity, and climate change,
770 *Proc. Natl. Acad. Sci. U.S.A.*, 115, 2305–2310, <https://doi.org/10.1073/pnas.1705349115>,
771 2018.

772 Sun, X., Tu, Y., Sun, S., Zhou, X., Jiang, L., Hao, X., Jiang, C., Gao, L.: Identification and
773 spatiotemporal characteristics of compound extreme climate events in the Minjiang River
774 Basin. *Water Resour. Hydropower Engineering (In Chinese)* 56 (3): 1-14. [https://](https://doi:10.13928/j.cnki.wrahe.2025.03.001)
775 doi:10.13928/j.cnki.wrahe.2025.03.001, 2025.

776 Talbot, C., Bou-Zeid, E., and Smith, J.: Nested Mesoscale Large-Eddy Simulations with WRF:
777 Performance in Real Test Cases, *J. Hydrometeorol.*, 13, 1421–1441,
778 <https://doi.org/10.1175/JHM-D-11-048.1>, 2012.

779 Tapiador, F. J., Navarro, A., Moreno, R., Sánchez, J. L., and García-Ortega, E.: Regional climate
780 models: 30 years of dynamical downscaling, *Atmos. Res.*, 235, 104785,
781 <https://doi.org/10.1016/j.atmosres.2019.104785>, 2020.

782 Tian, Y., Giaquinto, D., Di Capua, G., Claassen, J. N., Ali, J., Li, H., and De Michele, C.: Historical
783 changes in the Causal Effect Networks of compound hot and dry extremes in central Europe,
784 *Commun. Earth Environ.*, 5, 764, <https://doi.org/10.1038/s43247-024-01934-2>, 2024.

785 Torrez-Rodriguez, L., Goubanova, K., Muñoz, C., and Montecinos, A.: Evaluation of temperature
786 and precipitation from CORDEX-CORE South America and Eta-RCM regional climate
787 simulations over the complex terrain of Subtropical Chile, *Clim. Dyn.*, 61, 3195–3221,
788 <https://doi.org/10.1007/s00382-023-06730-w>, 2023.

789 Van Der Wiel, K. and Bintanja, R.: Contribution of climatic changes in mean and variability to
790 monthly temperature and precipitation extremes, *Commun. Earth Environ.*, 2, 1,
791 <https://doi.org/10.1038/s43247-020-00077-4>, 2021.

792 Varga, Á. J. and Breuer, H.: Sensitivity of simulated temperature, precipitation, and global radiation
793 to different WRF configurations over the Carpathian Basin for regional climate applications,
794 *Clim. Dyn.*, 55, 2849–2866, <https://doi.org/10.1007/s00382-020-05416-x>, 2020.

795 Varga, Á. J. and Breuer, H.: Evaluation of convective parameters derived from pressure level and
796 native ERA5 data and different resolution WRF climate simulations over Central Europe, *Clim.*
797 *Dyn.*, 58, 1569–1585, <https://doi.org/10.1007/s00382-021-05979-3>, 2022.

798 Wang, S., Chen, X., Yao, H., Ruan, W., Gu, Z., Li, X., Chen, Y., Liu, M., and Deng, H.: Separation
799 and spatial variations of typhoon and non - typhoon rainfall at different timescales in typical
800 region of southeast China, *Int. J. Climatol.*, 44, 4611–4628, <https://doi.org/10.1002/joc.8599>,
801 2024.

802 Wang, Y., Yang, K., Zhou, X., Chen, D., Lu, H., Ouyang, L., Chen, Y., Lazhu, and Wang, B.:
803 Synergy of orographic drag parameterization and high resolution greatly reduces biases of

804 WRF-simulated precipitation in central Himalaya, *Clim. Dyn.*, 54, 1729–1740,
805 <https://doi.org/10.1007/s00382-019-05080-w>, 2020.

806 Wu, H., Su, X., and Singh, V. P.: Increasing Risks of Future Compound Climate Extremes with
807 Warming Over Global Land Masses, *Earth's Future*, 11, e2022EF003466,
808 <https://doi.org/10.1029/2022EF003466>, 2023a.

809 Wu, J., Wang, Z., Dong, J., Cui, X., Tao, S., and Chen, X.: Robust Runoff Prediction with
810 Explainable Artificial Intelligence and Meteorological Variables From Deep Learning
811 Ensemble Model, *Water Resour. Res.*, 59, e2023WR035676,
812 <https://doi.org/10.1029/2023WR035676>, 2023b.

813 Wu, L. and Zheng, H.: Regional Climate Effects of Irrigation under Central Asia Warming by 2.0 °C,
814 *Remote Sens.*, 15, 3672, <https://doi.org/10.3390/rs15143672>, 2023.

815 Wu, X., Hao, Z., Zhang, X., Li, C., and Hao, F.: Evaluation of severity changes of compound dry
816 and hot events in China based on a multivariate multi-index approach, *J. Hydrol.*, 583, 124580,
817 <https://doi.org/10.1016/j.jhydrol.2020.124580>, 2020.

818 Wu, Y., Miao, C., Sun, Y., AghaKouchak, A., Shen, C., and Fan, X.: Global Observations and
819 CMIP6 Simulations of Compound Extremes of Monthly Temperature and Precipitation,
820 *GeoHealth*, 5, e2021GH000390, <https://doi.org/10.1029/2021GH000390>, 2021.

821 Xie, Y., Sun, W., Ren, M., Chen, S., Huang, Z., and Pan, X.: Stacking ensemble learning models
822 for daily runoff prediction using 1D and 2D CNNs, *Expert Syst. Appl.*, 217, 119469,
823 <https://doi.org/10.1016/j.eswa.2022.119469>, 2023.

824 Xu, W., Liu, Z., Gao, L., Lei, X., and Zhang, Y.: Changes in Global Marine Heatwaves in a Non -
825 stationary Climate, *Geophys. Res. Lett.*, 52, e2024GL114497,
826 <https://doi.org/10.1029/2024GL114497>, 2025.

827 Xu, Z., Han, Y., Tam, C.-Y., Yang, Z.-L., and Fu, C.: Bias-corrected CMIP6 global dataset for
828 dynamical downscaling of the historical and future climate (1979–2100), *Sci. Data*, 8, 293,
829 <https://doi.org/10.1038/s41597-021-01079-3>, 2021.

830 Yan, Y., Gao, L., Chen, R., Zhang, C., Ren, L., Zhang, X., Chen, C.: Analysis of Disaster and
831 Damage Process Caused by No. 2305 “Doksuri” Typhoon Disaster Chain in Fuzhou City. *J.*

832 Catastrophology (In Chinese) 39 (4): 228-234. [https://doi.org/10.3969/j.issn.1000-811X.2024.](https://doi.org/10.3969/j.issn.1000-811X.2024.04.033)
833 04. 033, 2024.

834 Yang, T., Chen, X., Hamdi, R., Li, Q., Cui, F., Li, L., Liu, Y., De Maeyer, P., and Duan, W.:
835 Assessment of snow simulation using Noah-MP land surface model forced by various
836 precipitation sources in the Central Tianshan Mountains, Central Asia, Atmos. Res., 300,
837 107251, <https://doi.org/10.1016/j.atmosres.2024.107251>, 2024.

838 Yang, T., Chen, X., Hamdi, R., Li, L., Cui, F., De Maeyer, P., and Duan, W.: Rainfall - Driven
839 Extreme Snowmelt Will Increase in the Tianshan and Pamir Regions Under Future Climate
840 Projection, J. Geophys. Res.: Atmos., 130, e2024JD042323,
841 <https://doi.org/10.1029/2024JD042323>, 2025a.

842 Yang, X., Yan, Y., Zhou, X., Zhu, L., Ma, M., Zhang, J., Chen, Y., and Gao, L.: Risk of Compound
843 Typhoon Disaster Chains: Insights from Southeastern China, Int. J. Disaster Risk Sci., 16,
844 870–887, <https://doi.org/10.1007/s13753-025-00674-x>, 2025b.

845 Yao, H., Zhao, L., He, Y., Dong, W., Shen, X., Wang, J., Hu, Y., Ling, J., Xiao, Z., and Huang, C.:
846 Changes caused by human activities in the high health-risk hot-dry and hot-wet events in China,
847 Commun. Earth Environ., 5, 464, <https://doi.org/10.1038/s43247-024-01625-y>, 2024.

848 Yin, C., Ting, M., Kornhuber, K., Horton, R. M., Yang, Y., and Jiang, Y.: CETD, a global compound
849 events detection and visualisation toolbox and dataset, Sci. Data, 12, 356,
850 <https://doi.org/10.1038/s41597-025-04530-x>, 2025.

851 Yin, H., Zhang, X., Wang, F., Zhang, Y., Xia, R., and Jin, J.: Rainfall-runoff modeling using LSTM-
852 based multi-state-vector sequence-to-sequence model, J. Hydrol., 598, 126378,
853 <https://doi.org/10.1016/j.jhydrol.2021.126378>, 2021.

854 You, J., Yin, F., and Gao, L.: Escalating wind power shortages during heatwaves, Commun. Earth
855 Environ., 6, 245, <https://doi.org/10.1038/s43247-025-02239-8>, 2025.

856 Zeng, J., Zhang, S., Zhou, S., Obulkasim, O., Zhang, H., Lu, X., and Dai, Y.: Comparison of the
857 risks and drivers of compound hot-dry and hot-wet extremes in a warming world, Environ.
858 Res. Lett., 19, 114026, <https://doi.org/10.1088/1748-9326/ad7617>, 2024a.

859 Zeng, J., Li, H., Sun, B., Chen, H., Wang, H., Zhou, B., and Duan, M.: Summertime compound heat
860 wave and drought events in China: interregional and subseasonal characteristics, and the

861 associated driving factors, *Environ. Res. Lett.*, 19, 074046, <https://doi.org/10.1088/1748->
862 9326/ad5576, 2024b.

863 Zhang, C., Wang, Y., and Hamilton, K.: Improved Representation of Boundary Layer Clouds over
864 the Southeast Pacific in ARW-WRF Using a Modified Tiedtke Cumulus Parameterization
865 Scheme*, *Mon. Weather Rev.*, 139, 3489–3513, <https://doi.org/10.1175/MWR-D-10-05091.1>,
866 2011.

867 Zhang, J., Zhao, T., Zhang, J., Ren, Y., and Li, Z.: Changes in compound temperature and
868 precipitation extremes from combined effects of multiple circulation factors over China, *J.*
869 *Hydrol.*, 642, 131884, <https://doi.org/10.1016/j.jhydrol.2024.131884>, 2024a.

870 Zhang, M., Han, Y., Xu, Z., and Guo, W.: Assessing Climate Extremes in Dynamical Downscaling
871 Simulations Driven by a Novel Bias - Corrected CMIP6 Data, *J. Geophys. Res.: Atmos.*, 129,
872 e2024JD041253, <https://doi.org/10.1029/2024JD041253>, 2024b.

873 Zhang, W., Luo, M., Gao, S., Chen, W., Hari, V., and Khouakhi, A.: Compound
874 Hydrometeorological Extremes: Drivers, Mechanisms and Methods, *Front. Earth Sci.*, 9,
875 673495, <https://doi.org/10.3389/feart.2021.673495>, 2021.

876 Zhang, W., Furtado, K., Wu, P., Zhou, T., Chadwick, R., Marzin, C., Rostron, J., and Sexton, D.:
877 Increasing precipitation variability on daily-to-multiyear time scales in a warmer world, *Sci.*
878 *Adv.*, 7, eabf8021, <https://doi.org/10.1126/sciadv.abf8021>, 2021.

879 Zhang, W., Zhou, T., and Wu, P.: Anthropogenic amplification of precipitation variability over the
880 past century, *Science*, 385, 427–432, <https://doi.org/10.1126/science.adp0212>, 2024.

881 Zhang, Y., Deng, C., Xu, W., Zhuang, Y., Jiang, L., Jiang, C., Guan, X., Wei, J., Ma, M., Chen, Y.,
882 Peng, J., and Gao, L.: Long-term variability of extreme precipitation with WRF model at a
883 complex terrain River Basin, *Sci. Rep.*, 15, 156, <https://doi.org/10.1038/s41598-024-84076-x>,
884 2025.

885 Zhao, T., Xiong, S., Tian, Y., Wu, Y., Li, B., and Chen, X.: Compound dry and hot events over major
886 river basins of the world from 1921 to 2020, *Weather Clim. Extremes*, 44, 100679,
887 <https://doi.org/10.1016/j.wace.2024.100679>, 2024.

888 Zheng, M., Chen, X., Ruan, W., Yao, H., Gu, Z., Geng, K., Li, X., Deng, H., Chen, Y., and Liu, M.:
889 Spatiotemporal variation of water cycle components in Minjiang River Basin based on a

890 correction method for evapotranspiration products, *J. Hydrol.: Reg. Stud.*, 50, 101575,
891 <https://doi.org/10.1016/j.ejrh.2023.101575>, 2023.

892 Zhou, P., Tang, J., Ma, M., Ji, D., and Shi, J.: High resolution Tibetan Plateau regional reanalysis
893 1961-present, *Sci. Data*, 11, 444, <https://doi.org/10.1038/s41597-024-03282-4>, 2024.

894 Zscheischler, J., Westra, S., Van Den Hurk, B. J. J. M., Seneviratne, S. I., Ward, P. J., Pitman, A.,
895 AghaKouchak, A., Bresch, D. N., Leonard, M., Wahl, T., and Zhang, X.: Future climate risk
896 from compound events, *Nature Clim. Change*, 8, 469–477, [https://doi.org/10.1038/s41558-](https://doi.org/10.1038/s41558-018-0156-3)
897 018-0156-3, 2018.